doi:10.1038/nature111063

1. Superflares on G-type main sequence stars and previous large surveys

In case of our Sun, the amplitude of brightness change by white-light flares is order of 0.01% of the total brightness of the Sun[10] even in case of the largest solar flare that occurs once in 10 years. The amplitude of brightness change by the white-light flares on solar-type stars is small and the occurrence frequency of large flares thought to be extremely low. Moreover, the duration of the white-light flares on the Sun and other late-type main sequence stars is typically less than a few hours. Several large surveys (e.g. OGLE[30], MACHO[31], and ASAS[32]) have been accumulating an awesome coverage and even very rare events like large-amplitude superflares on solar-type stars might be recorded in their data. However the time cadence of these surveys is completely inappropriate for picking out superflares and it is difficult to distinguish between the real superflares and the false events. The detection of white-light flares on solar-type stars requires high photometric precision with continuous time series data of a large number of stars over a long period. The Kepler satellite is useful to detect the small increase in the stellar brightness due to stellar flares[33].

2. Flare detection

We analyzed the long-cadence calibrated flux (time resolution of 29.4 min) for 52,496, 156,097, 165,470, and 5,295 stars in the data of the quarters 0, 1, 2, and 3 respectively which were taken by the Kepler satellite from 2009 April to 2009 December. These data were retrieved from the Multimission Archive at STScI (MAST). We created light curves for all stars from the corrected flux in the data[34,35], and searched for the sudden brightenings. The distribution of brightness changes between all pairs of 2 consecutive data points was first calculated. We then picked up 'superflares', placing the threshold of the flare at three times of the value at the top 1% of this distribution. The typical value of this threshold is about 0.1% of the brightness of the star. On G-type main sequence stars, this roughly corresponds to the peak bolometric luminosity of 9×10^{29} erg/s and the total released energy of 3×10^{33} erg if the flare duration is 1 hour (Note that the time resolution of 29.4 min hinders us from finding flares with the duration shorter than 1 hour). This is about 10 times more energetic than the largest solar flare observed so far. We defined the time at which the flux first exceeds the threshold as the flare start time. After removing the long-term brightness variation except for the data around flare candidates, we estimated the flare duration. The flare end time was defined to be the time at which the flux residuals become smaller than the threshold. We analyzed only flares with the duration longer than 0.05 days (at least 2 consecutive data points must exceed the threshold).

In order to exclude the contribution from flares on neighboring stars, we excluded flares which occurred on the G-type main sequence stars with neighboring stars within 12 arc seconds. Since the typical photometric aperture contains about 30 pixels[34], we assumed that the aperture radius is 3 pixels = 12 arc seconds. Moreover, we excluded pairs of flares which occurred at the same time and whose distance is less than 24 arc-

seconds. About 68 percent of the detected flares on G-type main sequence stars were excluded by these conditions. We selected 389 flares on 161 G-type main sequence stars.

After removing the candidates of neighboring flares, we examined the pixel level data of each G-type main sequence stars showing flares. Figure S1 shows an example of the light curve and the pixel count variation around a flare on KIC 11401109. The sudden increase in pixel counts occurred at the same cadence of the flare and only pixels correspond to the point spread function (PSF) of the target show the increase of pixel counts. On the other hand, figure S2 shows an example of the false event light curve and the pixel counts variation on KIC 7189661. Although the sudden increase in pixel count occurred at the same cadence of the flare, the PSF and the position of the flare component are not consistent with those of the target. We compared the position and the PSF shape of the target to those of the flare component and excluded 24 false events. Finally we selected 365 flares on 148 G-type main sequence stars for further analysis.

3. Occurrence frequency of superflares

We estimated the average occurrence frequency of superflares from the number of superflares, the number of observed stars, and the length of the observation period. Since we excluded the superflares on the G-type main sequence stars with neighboring stars within 12 arc seconds, we also excluded the G-type stars which have neighboring stars within 12 arc seconds from the population of G-type stars. The numbers of G-type main sequence stars that we used for the flare-frequency calculation are 3,378 (Q0), 26,412 (Q1), 29,259 (Q2) and 1,919 (Q3) respectively. The lengths of the observation period of each quarter are 10 days (Q0), 33 days (Q1), 90 days (Q2) and 90 days (Q3). The occurrence frequency in unit energy range (f) can be estimated from the number of flares (N_{flares}), the total population of stars (N_{star}), the length of the observation period (τ_{obs}), and the bin width (ΔE_{flare}) by the equation (S1):

$$f = \frac{N_{flares}}{N_{stars} \cdot \tau_{obs} \cdot \Delta E_{flare}} \qquad \text{(S1)}.$$

For example, the number of superflares on slowly rotating (P>10 days) and higher temperature G-type main sequence stars with the total energy between 3.2×10^{34} erg and 5.6×10^{34} erg is 3 and the numbers of slowly rotating and higher temperature stars for each quarter are 1,923, 12,524, 13,851, and 1,112 respectively. Hence the occurrence frequency can be derived to be 2.5×10^{-38} erg^{-1} year^{-1}.

We estimated the total energy of each flare from stellar luminosity, amplitude and duration of flares. The stellar luminosity was estimated from the stellar radius and the surface temperature in the Kepler Input Catalog. According to Brown et al.[9], 1σ uncertainties of the stellar radius and the surface temperature in the Kepler Input Catalog are about ±0.2 dex and ±200K respectively. Hence the uncertainty in the stellar luminosity can be estimated to be about ±60%. Although the time-cadence of the Kepler data was not sufficiently short to determine the peak and duration of flares, the uncertainties of the amplitude and duration of flares are much smaller than the

uncertainty in the stellar luminosity because, when we calculate the flare energy, we integrate the brightness variation due to the flare over time from the start to end of the flare. Therefore total uncertainty in the flare energy is about ±60% and the occurrence frequency of superflares in unit energy range includes not only the counting error (the square root of the number of flares) but also the uncertainty of the flare energy.

4. Brightness variations

Most of G-type main sequence stars showing superflares show quasi-periodic brightness variations. The period of the brightness variation was estimated by the discrete Fourier transform (DFT) method. After removal of linear trends and adjustment of gaps in flux between each quarter, we computed a periodogram for each star with a range of the period between 0.1 days to half the data length (typically about 60 days). We determined the period with the highest peak (with an amplitude $\geqq 10^{-4}$ of the average brightness) was the variation period of the star.

Figures S3 a and b show the DFT spectrum and long-term light curve of KIC 6034120. In figure S3 b, the top and bottom panels represent the DFT spectrum of observed data and that of the single-period artificial data respectively. We generated an artificial single-period sinusoidal light curve with the same time sampling as the observed data. Around the frequency of the largest amplitude component, the DFT spectrum of the observed light curve is slightly wider than that of the single-period artificial light curve. Figure S3 c shows a light curve of KIC 6034120 folded by the best estimated period of 5.69 days. The large scatter of the data in the folded light curve indicates that the coherence of the brightness variation is low. These properties suggest that the brightness modulations of KIC 6034120 are not caused by the orbital motion of the binary system, but the differential rotation of the star with multiple starspots or changes in the shape and size of starspots. Of course, we could not exclude the possibility of an active binary system which has large starspots. More detailed observations and analysis (e.g. high-dispersion spectroscopy) are necessary to reveal the nature of each superflare star.

5. Flare frequency and the effective temperature of the stars

Figure S4 shows the occurrence frequency of superflares as a function of the effective temperature. Since the luminosity of the stars decreases as the temperature of the star decreases, the detection limit of flares on the lower-temperature stars will be smaller than that of flares on the higher-temperature stars. In order to exclude the bias due to the detection limit, we used only flares with the energy $\geqq 5\times10^{34}$ erg. As discussed in the main text, the occurrence frequency of superflares depends on the effective temperature of the stars, and the frequency increases as the temperature decrease. The occurrence frequency of superflares on G-type stars with the temperature range between 5,600 and 6,000K is about 1/4 of that of superflares on stars with the temperature range between 5,100 and 5,600K. For slowly rotating G-type main sequence stars, the occurrence frequency on higher-temperature G-type stars is about 1/10 of that on lower-temperature

G-type stars.

6. Starspots and superflares

The energy sources of solar and stellar flares are thought to be the magnetic energy stored near the sunspot or starspot[11]. In this case, the total energy released by the flare must be smaller than (or equal to) the stored magnetic energy. The order of the stored magnetic energy (E_{mag}) can be roughly estimated by

$$E_{mag} \approx \frac{B^2 l^3}{8\pi} \quad \text{(S2)}$$

where B and l correspond to the magnetic field strength and the size of the starspot region.

Starspots can cause brightness variations by the rotation of the star. It is known that our Sun shows fluctuations in brightness due to sunspots[10]. Late-type stars showing quasi-periodic brightness variations due to the rotation of the star with starspots are known as BY Dra type variable stars[11]. If there is a starspot or a starspot group with the area of A_{spot} and the temperature of T_{spot} on the surface of the star with the apparent area of A_{star} and the effective temperature of T_{star}, the full-amplitude of the rotational brightness variation normalized by the average brightness (ΔF_{rot}) can be estimated by

$$\Delta F_{rot} \approx \left[1-\left(\frac{T_{spot}}{T_{star}}\right)^4\right]\frac{A_{spot}}{A_{star}}. \quad \text{(S3)}$$

Since the Kepler photometer covers a wide spectral rage (from 400 nm to 850 nm), observed brightness changes would be nearly equal to the bolometric brightness change obtained by the equation S3.

If we assume that $l^3 = A_{spot}^{3/2}$, the equation S2 can be transformed to

$$E_{mag} \approx \frac{B^2}{8\pi} A_{spot}^{3/2} \approx \frac{B^2}{8\pi}\left(\frac{A_{star}\Delta F_{rot}}{1-\left(T_{spot}/T_{star}\right)^4}\right)^{3/2} \geq E_{flare} \quad \text{(S4)}$$

where E_{flare} is the total energy released by the flare.

The amplitude of the flare normalized by the average brightness (ΔF_{flare}) can be estimated by

$$\Delta F_{flare} \approx \frac{E_{flare}}{L_{star}\tau} \quad \text{(S5)}$$

where L_{star} is the luminosity of the star and τ is the e-folding time of the flare. Then the relation between the flare amplitude and the brightness variation amplitude can be written as

$$\Delta F_{flare} \approx \frac{B^2}{8\pi}\frac{A_{spot}^{3/2}}{L_{star}\tau} \approx \frac{B^2}{8\pi}\frac{1}{L_{star}\tau}\left(\frac{A_{star}\Delta F_{rot}}{1-\left(T_{spot}/T_{star}\right)^4}\right)^{3/2} \propto A_{spot}^{3/2} \propto \Delta F_{rot}^{3/2} \quad \text{(S6)}.$$

This indicates that the flare amplitude is proportional to 1.5 power of the area of starspots. If we adopt $L_{star}=10^{33}$ erg/s,$\tau=10^4$sec, T_{spot}=4,000K and T_{star}=6,000K for

superflares on G-type main sequence stars, then the flare amplitude can be roughly estimated by

$$\Delta F_{flare} \approx 10^{-2}\left(\frac{B}{1000G}\right)^2\left(\frac{r_{spot}}{0.1R_{sun}}\right)^3 \approx 10\left(\frac{B}{1000G}\right)^2 \Delta F_{rot}{}^{3/2}, \qquad \text{(S7)}$$

where r_{spot} and R_{sun} correspond to the radius of the starspot and the solar radius respectively.

Figure S5 a shows the scatter plot of the flare amplitude as a function of the full-amplitude of brightness variation. We defined the amplitude of brightness variation as the normalized brightness range, in which the lower 99 percent of the distribution of brightness difference from the average, except for the flares, are included. As for B=1,000 G, the analytic relation between the flare amplitude and the variation amplitude obtained from equation S7 is shown as a solid line in figure S5 a. Many of the flares have smaller amplitudes than that expected by the equation S7. This suggests that the order of energy released by these flares can be explained by the magnetic energy stored near the starspots. However some flares have larger amplitudes than expected from the equation S7. This can be explained by the inclination of the star, i, where i is the angle between the line of sight and the rotation axis of the star. In stars with lower inclination angle, the amplitude of brightness variation is smaller. All flares have smaller flare amplitudes than that expected in the nearly pole-on case (dashed-line; i=2 degree). A similar relation between the solar flare energy and the sunspot area is known[36].

Figure S5 b shows the frequency distribution of flares as a function of the amplitude of brightness variation. More frequent flares tend to be observed on stars with larger brightness variation. This indicates that more frequent flares occur on stars with a larger total area of starspots.

As shown in figure 3 b, slowly rotating stars have a lower frequency of flares than rapidly rotating stars. The flare frequency on slowly rotating stars is about 1/4 of that on rapidly rotating stars. However, figure S5 a and b indicate that a large starspot can appear and large amplitude superflares can occur on slowly rotating G-type main sequence stars.

Figure S6 exhibits a light curve of superflares on slowly rotating Sun-like stars, KIC 11764567. This star shows brightness variations with an amplitude of about 2 percent and a period of 22.7 days. If we assume that the brightness variation is caused by the rotation of the star with starspots and the inclination angle of the star is nearly edge-on (i~90 degree), starspots on this star cover 2.5 percent of its surface, though the rotation period of this star is close to that of the present Sun. This star is an example of the slowly rotating G-type main sequence stars like our present Sun which produce large starspots and superflares.

7. On the possibility of superflares on low-temperature secondary stars

According to our preliminary analysis of superflares on M-type and K-type main

sequence stars using the Kepler data (Maehara et al. 2012, in preparation), the occurrence frequency of superflares on K- and M-type stars is much higher than that of superflares on G-type main sequence stars. For superflares with the energy of 10^{35} erg, the average frequencies of such superflares on K- and M-type stars are about 5 and 20 times higher than that of superflares on G-type stars. If a low-activity G-type main sequence star like our Sun has an active M-type secondary star, such binary star would look like a superflare-generating solar-type star. The fraction of superflare stars for G-type main sequence stars is about 0.5 % (148 flare stars in 29,510 G-type stars) and that for the M-type main sequence stars is about 14 % (86/613). Therefore, if we assumed that all of superflare-generating solar-type stars have active M-type secondary stars and all superflares occurred on M-type secondary stars, about 4% of G-type main sequence stars must have M-type companions. Since the binary fraction of G-type main sequence stars with the mass ratio < 0.3 is about 20 %[37], the possibility of the superflares on active M-type secondary stars could not be excluded. However the positive correlation between the amplitude of stellar brightness modulations and the flare frequency shown in Figure S5 b could not be explained by the M-type companion scenario. The brightness variation of G-type stars with the amplitude of 1% could not be explained by only the large starspots on active M-type stars because of following reasons; (1) the G-type stars are about 100-1,000 times brighter than the M-type main sequence stars, (2) the temperature difference between the quiet region of the star and the starspots decreases as the surface temperature of the star decreases[38]. Hence even the large starspots on the M-type companions could not produce large amplitude modulations of the total luminosity.

In the case of a binary star which consists of a G-type star and a K-type star, the brightness variation amplitude could be explained by large starspots on active K-type secondary. Since the fraction of flare stars for K-type stars is about 3% (240 flare stars in 8,295 K-type stars), if we assume that all superflares occurred on the K-type secondary stars, about 15% of G-type main sequence stars must have K-type companions. The binary fraction of nearby G-type stars with the mass ratio between 0.4 and 0.8 was estimated to be about 10 %[37] and this value is comparable to the binary fraction estimated from the flare star fraction. However the dependence of the flare occurrence frequency on the surface temperature of stars (figure S4) could not be explained by the binary scenario with K-type companions. If all superflares occur on the low-temperature companions, the occurrence frequency does not depend on the surface temperature of primary stars. Although we cannot completely exclude the possibility that superflares occur on unseen binary companion, we can say that at least some of superflares should occur on G type main sequence stars since there is an empirical correlation between surface temperature of G type main sequence stars and occurrence frequency of superflares (figure S4).

8. Contribution from the flares on neighboring stars

We excluded superflares on G-type stars which have neighboring stars from the analysis in order to remove flares on nearby faint stars. We used the Kepler Input Catalog[9] to determine whether there is no neighboring star within the photometric aperture. However, because of the detection limit of the Kepler Input Catalog, we could not exclude the possibility of flares on un-cataloged stars. Here we estimate the number of flares which occurred on un-cataloged faint stars.

Figure S7 shows the distribution of the number of stars per square arcsec as a function of the relative brightness of the stars against a 15-mag star. The number of stars increases as the brightness of the stars decreases. If we assume that the number density of stars increases as a power-law of the brightness of stars (dotted-line in figure S7a), the number of the 20-mag stars (1/100 of the brightness of a 15-mag star) within the photometric aperture (typically 480 arcsec^2 for a 12-mag star) is about 2. A flare with the amplitude of 100% on a nearby 20-mag star could produce a flare-like brightening with the amplitude of 1 % on the 15-mag star. According to the occurrence frequency distribution of superflares on M-type stars which more frequently show flares, the frequency of flares with the amplitude of 100% is 4×10^{-5}/year/star (figure S7 b). The number of solar-type stars we used for the analysis is about 30,000 and the length of observation period is about 120 days, hence the number of flares on nearby stars can be estimated to be about 0.8. This value is much smaller than the total number of superflares on G-type main sequence stars, 365. The number density of stars increases as the brightness of the stars decreases with an exponent 1.8. On the other hand, the occurrence frequency of flares decreases as the flare amplitude increases with an exponent about -1.8. Therefore the contribution from the flares on faint neighboring stars is estimated to be less than the order of 1% of the total number of flares on G-type stars and is negligible.

9. Hot Jupiter and superflares

Rubenstein & Schaefer (2000)[7] proposed that superflares on ordinary solar-type stars are caused by magnetic reconnection between the magnetic fields of the primary star and a gas-giant planet orbiting close to the star by analogy with the high magnetic activity of RS CVn binary systems. RS CVn stars are a class of binary systems with the orbital period between 1 and 14 days consisting of a F- or G-type main sequence star as a hotter component. The hotter component of the binary is tidally spun up by the close companion and shows high magnetic activity[39]. It is known that RS CVn systems show large flares[40] and they are thought to be caused by magnetic reconnection mediated by the close companion star[41].

Cuntz et al.[26] discussed that stellar activity would be enhanced due to the two types of star-planet interaction; one is the tidal interaction and the other is the magnetic interaction. Both interactions strongly decrease with the distance between the host star and planet.

Shkolnik et al. reported chromospheric activity related to the hot Jupiter on HD179949

and ν And[42,43]. For both stars, the cyclic variation of the intensity of CaII K line synchronized to the hot Jupiter's orbit was observed. Lanza[44] reported that the phase-difference between the chromospheric hot spot and the hot Jupiter could be explained by the magnetohydrostatic model.

Ip et al.[27] performed numerical simulations using a resistive MHD code in order to investigate the interaction of the magnetosphere of hot Jupiters with the host stars. They reported that the flare energy of the same order of magnitude as that of a typical solar flare could be generated by the magnetic interaction between the magnetosphere of hot Jupiters and the host stars.

According to Borucki et al.[28], 1,235 planet candidates have been discovered around 997 host stars from 156,453 stars. We checked the list of planet candidates. In the case of a hot Jupiter orbiting around a solar-type star, the probability of transits averaged over all possible orbital inclinations is about 10%[45]. Since the majority of hot Jupiters has already detected by the Kepler planetary transit search[29], about 15 solar-type stars showing superflares should be identified as planet-hosting stars if we assume all superflares on 148 solar-type stars are caused by hot Jupiters. However, no planet has been found around 148 G-type main sequence stars showing superflares in our samples. As discussed in the previous section, the frequency of superflares increases as the amplitude of the rotational brightness variations increases. These brightness variations may prevent the detection of planetary transits. Although we could not completely exclude the possibility of selection bias, the non-detection of planetary transits suggests that hot Jupiters associated with superflares are rare.

Supplementary References

30. Udalski, A., Szymanski, M., Kaluzny, J., Kubiak, M., and Mateo, M. The Optical Gravitational Lensing Experiment. *Acta Astronomica* **42**, 253-284 (1992)
31. Alcock, C. et al., The search for massive compact halo objects with a (semi) robotic telescope in Robotic telescopes in the 1990s (ed. Fillippenko, A.V.) , *Astr. Soc. Pacif. Conf. Ser.*. **34**, 193-202 (1992)
32. Pojmanski, G. The All Sky Automated Survey. Catalog of Variable Stars. I. 0 h - 6 h Quarter of the Southern Hemisphere. *Acta Astronomica* **52**, 397-427 (2002)
33. Walkowicz,L,M., et al. White-Light Flares on Cool Stars in the Kepler Quarter 1 Data. *Astron. J.* **141**. doi:10.1088/0004-6256/141/2/50 (2011)
34. Van Cleve, J. E. and Caldwell, D. A. Kepler Instrument Handbook. KSCI-19033 (2009)
35. Fraquelli, D. and Thompson, S. E. Kepler Archive Manual. KDMC-10008-002 (2011)
36. Sammis, I., Tang, F., and Zirin, H. The Dependence of Large Flare Occurrence on the Magnetic Structure of Sunspots. *Astrophys. J.* **540**, 583-587 (2000)
37. Duquennoy, A. and Mayor, M. Multiplicity among solar-type stars in the solar neighbourhood. II - Distribution of the orbital elements in an unbiased sample. *Astron. Astrophys.* **248**, 485-524 (1991)
38. Berdyugina, S. V. Starspots: A Key to the Stellar Dynamo. *Living Reviews in Solar Physics* **2**, 8 (2005)
39. Walter, F. M.; Bowyer, S. On the coronae of rapidly rotating stars. I - The relation between rotation and coronal activity in RS CVn systems. *Astrophys. J.* **245**, 671-676 (1981)
40. Tsuru, T. et al. X-ray and Radio Observations of Flares from the RS Canum Venaticorum System UX Arietis. *Publications of the Astronomical Society of Japan* **41**, 679-695 (1989)
41. Simon, T., Linsky, J. L.,and Schiffer, F. H., III *IUE* SPECTRA OF A FLARE IN THE RS CANUM VENATICORUM-TYPE SYSTEM UX ARIETIS. *Astrophys. J.* **239**, 911-917 (1980)
42. Shkolnik, E., Walker, G. A. H., and Bohlender, D. A. EVIDENCE FOR PLANET-INDUCED CHROMOSPHERIC ACTIVITY ON HD 179949. *Astrophys. J.* **598**, 1092-1096 (2003)
43. Shkolnik, E., Walker, G. A. H., Bohlender, D. A., Gu, P.-G., and Kürster, M. HOT JUPITERS AND HOT SPOTS; THE SHORT- AND LONG-TERM CHROMOSPHERIC ACTIVITY ON STARS WITH GIANT PLANETS. *Astrophys. J.* **622**, 1075-1090 (2005)
44. Lanza, A. F. Hot Jupiters and stellar magnetic activity. *Astron. Astrophys.* **487**, 1163-1170 (2008)
45. Kane, S. R., von Braun, K. Constraining Orbital Parameters through Planetary

Transit Monitoring. *Astrophys. J.* **689**, 492-498 (2008)

Supplementary Figures

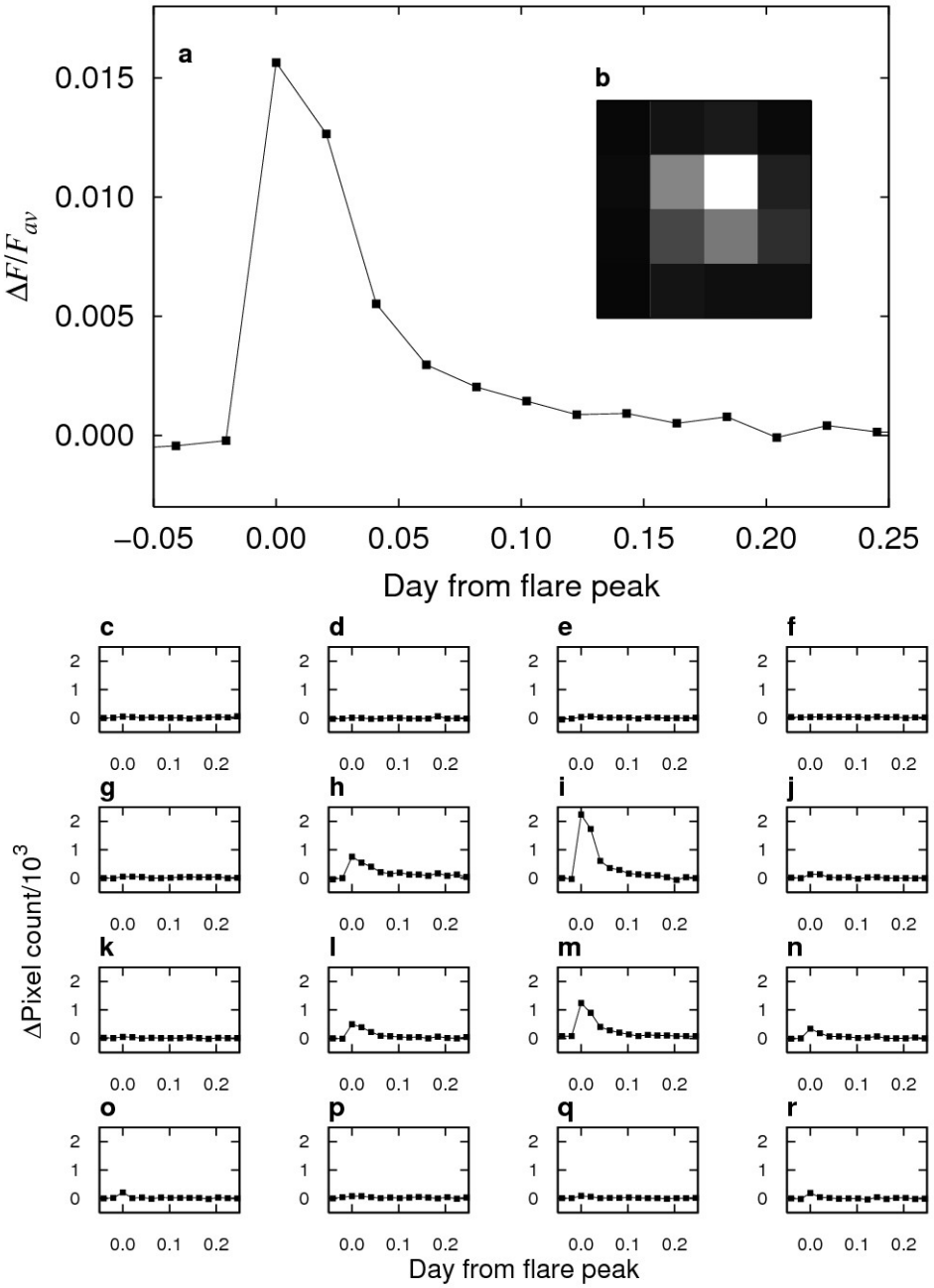

Figure S1. Light curve and each pixel count variation of a superflare on KIC 11401109.

a, Light curve of the superflare. The vertical axis represents the normalized difference between observed brightness during each cadence and the average brightness during the observation period. The horizontal axis represents the time from the flare peak.

b, Pixel image of KIC 11401109 around the superflare. The brightness of each pixel corresponds to the total count of each pixel.

c-**r**, Pixel-count variation of each pixel. The arrangement of these 16 panels corresponds to the position of each pixel shown in b. The vertical axis represents the pixel-count difference from the non-flare level in units of 1,000, and the horizontal axis represents the time from the flare peak. These figures show that observed superflare occurred on the target.

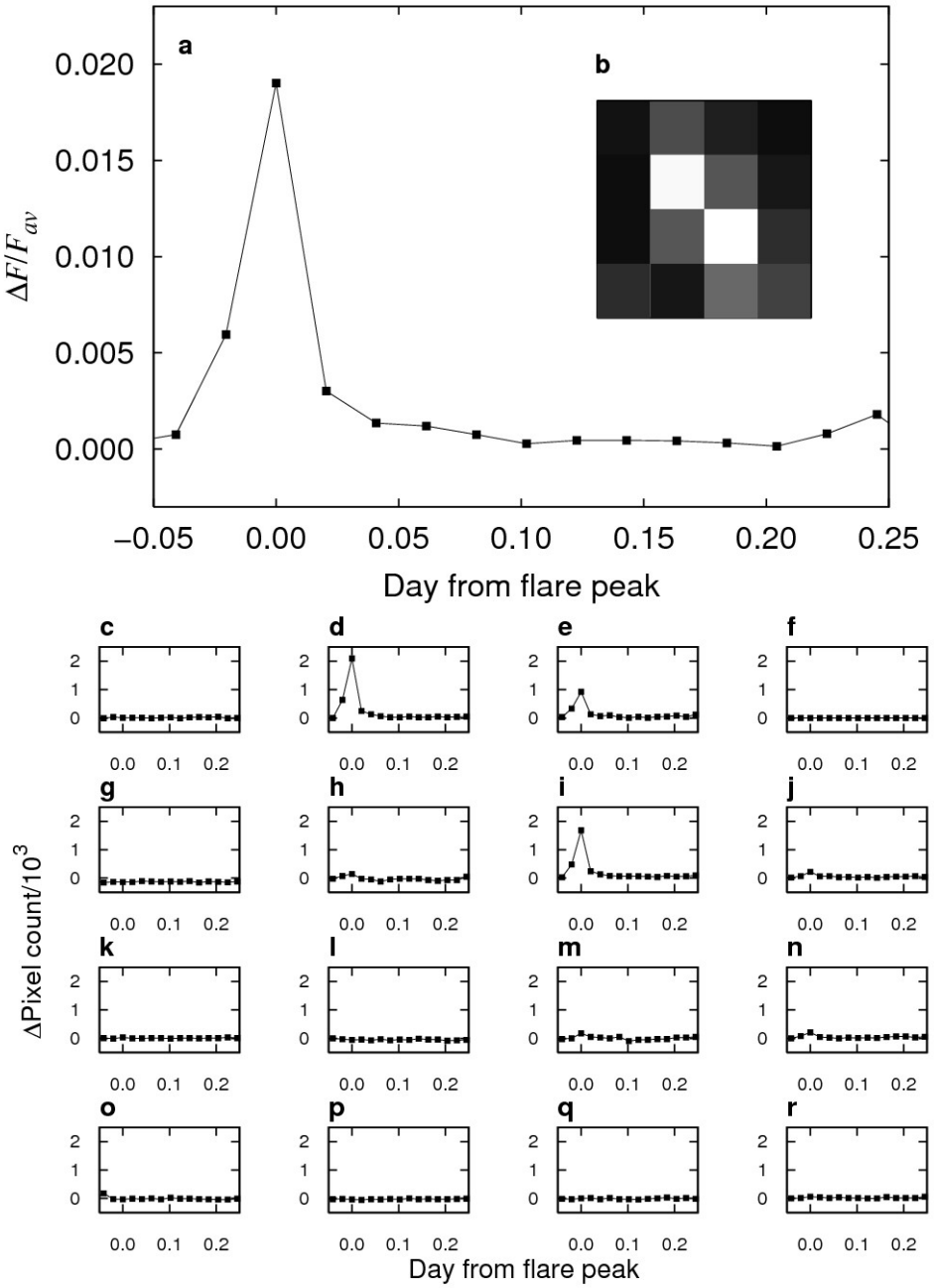

Figure S2. Same as figure S1, but for a false event on KIC 7189661.
Sudden increases in pixel count were recorded at pixels correspond to d, e, and i.

However these pixels were not consistent with the position of the target. These figures show that the flaring object is not the target but a near neighbor. These false events were excluded for the analysis.

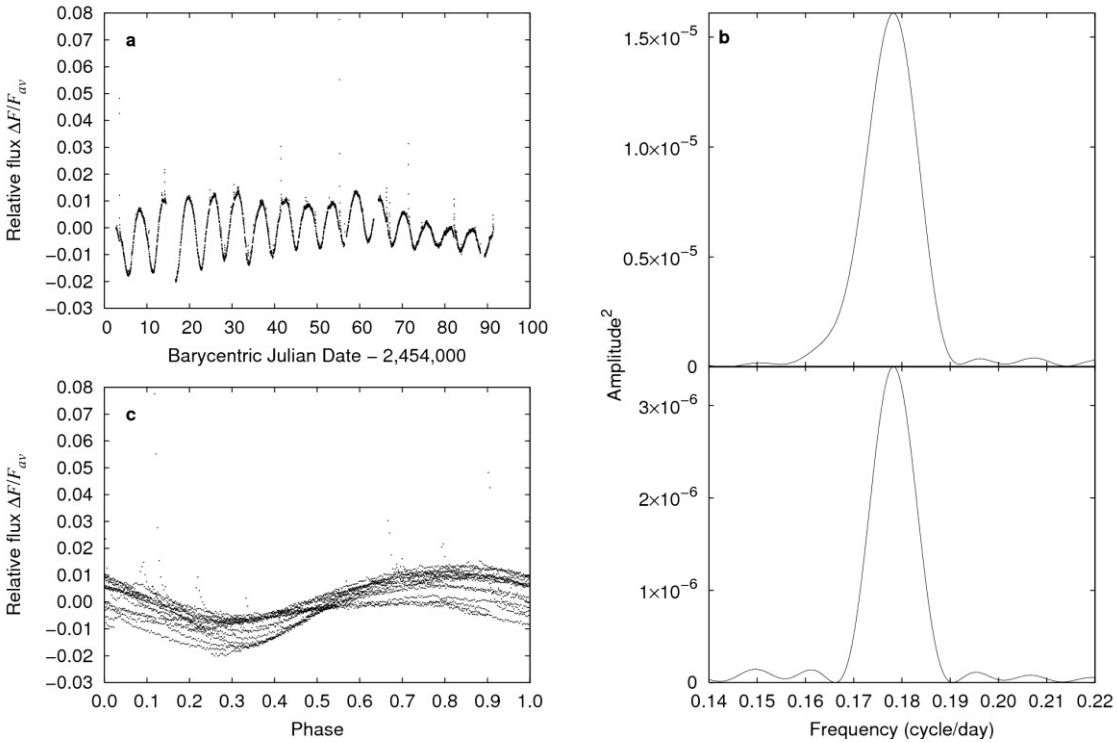

Figure S3. Quasi-periodic brightness modulation in KIC 6034120.
a Long-term light curve of KIC 6034120.
b Top: The DFT spectrum of observed data shown in **a**. Bottom: same as the top panel but for a single-period sinusoidal light curve with the same time sampling of the observed data.
c Light curve of KIC 6034120 folded on the best-estimated period of 5.69 days. The horizontal axis means the modulation phase which was taken arbitrarily.

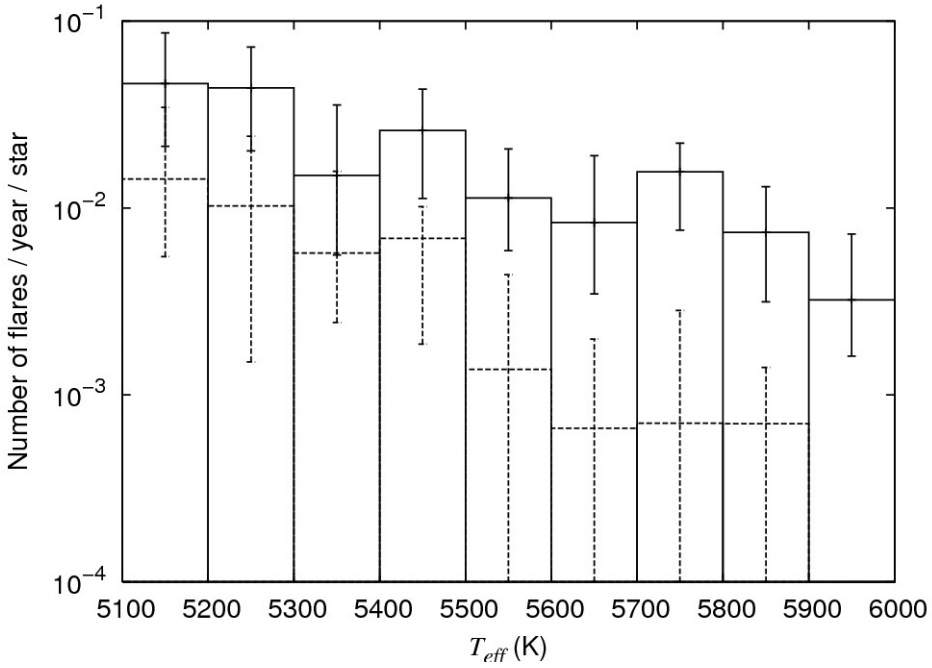

Figure S4. Distribution of the flare occurrence frequency as a function of the effective temperature of the stars.

These histograms show the frequency distribution of flares with the energy $\geqq 5\times10^{34}$ erg on all G-type main sequence stars (solid line) and on slowly rotating G-type main sequence stars (dashed line; excluding the stars showing quasi-periodic brightness modulations with periods shorter than 10 days). The vertical axis represents the number of flares per star per year in each temperature bin (100 K). The error bars represents the 1σ uncertainty estimated from the uncertainty in the energy estimation and the square root of event number in each period bin. The occurrence frequency of flares decreases as the effective temperature increases. The occurrence frequency of flares on the late G-type stars is about 5 times higher than that of flares on the early G-type stars.

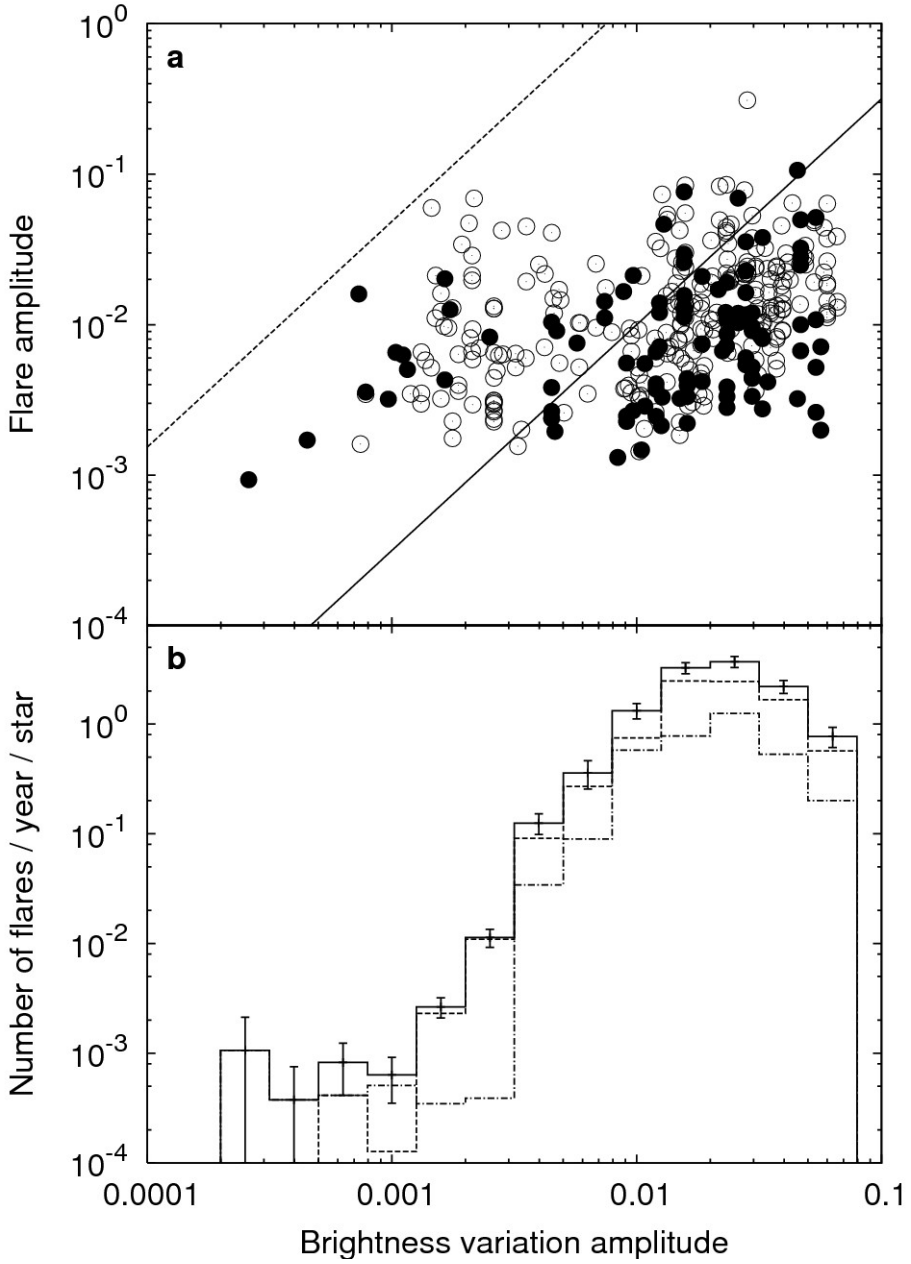

Figure S5. Relations between the brightness variation amplitude and the properties of superflares on G-type main sequence stars.

a, Scatter plot of flare amplitude as a function of brightness variation amplitude. Open circles and filled circles correspond to flares on rapidly rotating (period < 10 days) and those on slowly rotating (period ≧ 10 days) G-type main sequence stars respectively. Solid line corresponds to the analytic relation between the variation amplitude and flare amplitude obtained from equation S6. The dashed line corresponds to the same relation in case of nearly pole-on (i=2.0 deg).

b, Distribution of the flare occurrence frequency as a function of the brightness variation amplitude. The vertical axis represents the number of flares per star per year in

each amplitude bin. The histogram with a solid line corresponds to the occurrence frequency distribution of flares on all G-type main sequence stars. The error bars represent the square root of the event number in each bin. The dashed line and dash-dotted line correspond to the occurrence frequency distribution of flares on rapidly rotating and that of flares on slowly rotating G-type main sequence stars.

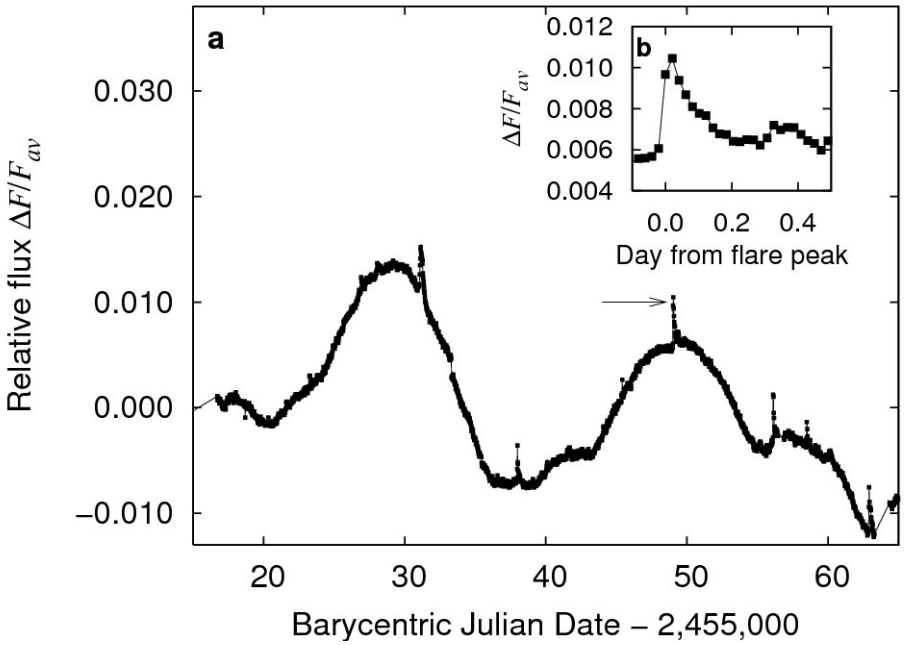

Figure S6. Light curve of superflares on a slowly rotating G-type main sequence star KIC 11764567.

a, Long-term light curve from BJD 2,4550,015 to 2,550,065. The individual points represent the difference between observed brightness during each cadence and the average brightness during the observation period.

b, Enlarged light curve of a superflare observed at BJD 2,455,024.95.

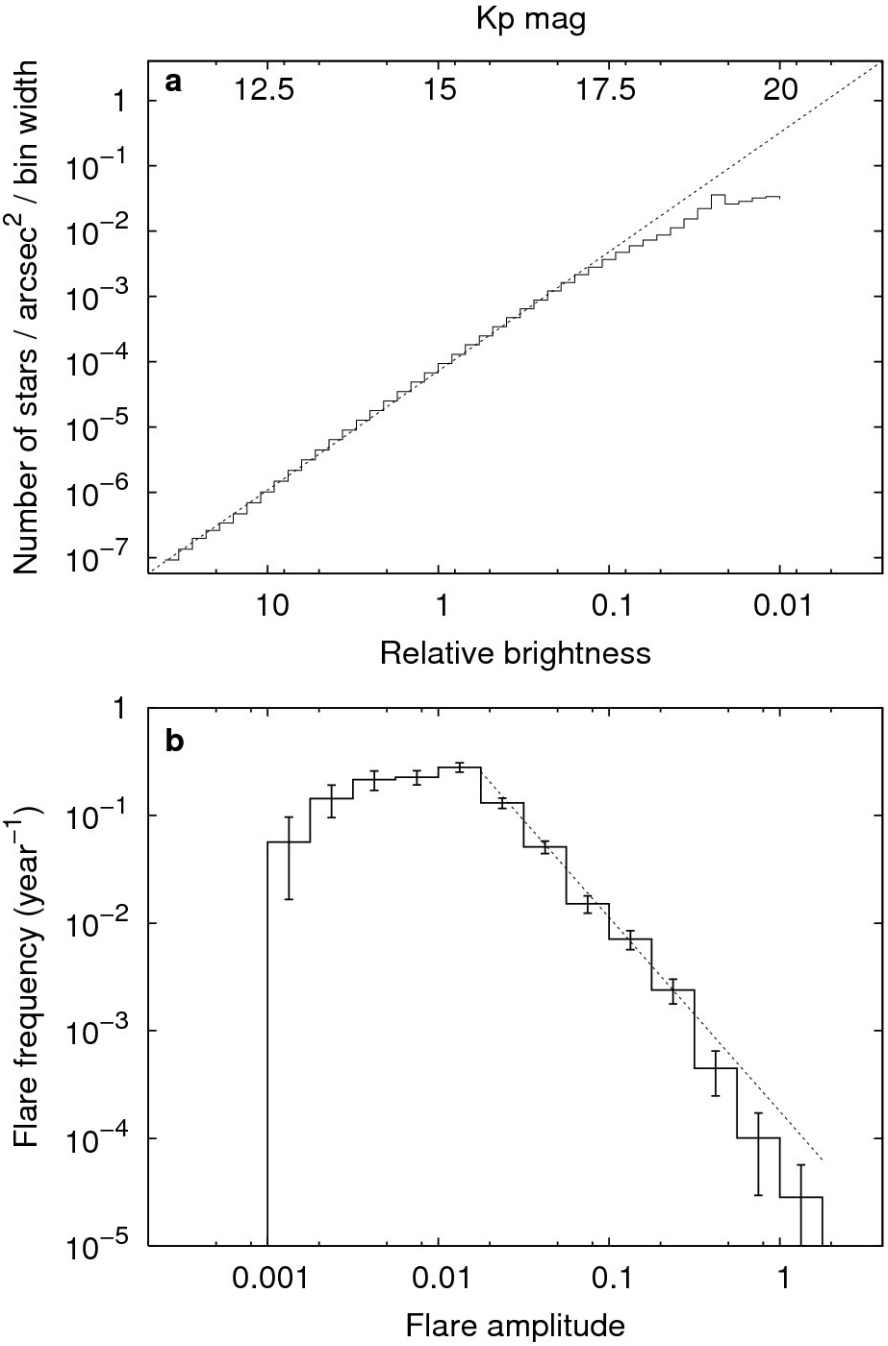

Figure S7. The comparison between the number density distribution of stars in the Kepler field and the frequency distribution of superflares.
a, The distribution of the number of stars per arcsec^2 as a function of the relative brightness of stars. The lower horizontal axis represents the relative brightness of stars against a 15-mag star and the upper horizontal axis represents the Kp magnitude of stars. The vertical axis is the number of stars per 1 arcsec^2 per bin width. The solid-line histogram shows the distribution of the number density of stars in the Kepler Input Catalog. The dashed-line shows the power-law fit for the bright-end of the sample (Kp

mag < 17). The power-law index is -1.8±0.1.
b, The frequency distribution of superflares on M-type stars as a function of the flare amplitude (solid-line histogram). The horizontal axis represents the amplitude of flares and the vertical axis means the number of flares per star, per year, and per unit amplitude. The error bars represent the square root of event number in each bin. The dashed-line shows the power-law fit for the frequency of the flares in the large-amplitude regime (amplitude≧0.02). The power-law index is -1.8±0.1.

Appendix I: List of G-type main sequence stars showing superflares

Table S1: List of G-type main sequence stars showing superflares

KPID	$T_{\rm eff}$[1]	$\log g$[1]	g mag.[1]	Period[2]	Amplitude[3]	N[4]	Flare rate (d^{-1})
2158047	5124	4.3	14.60	5.35	3.54×10^{-3}	1	8.2×10^{-3}
2303352	5348	4.7	14.97	3.04	1.86×10^{-4}	1	8.2×10^{-3}
2860579	5162	4.5	14.85	5.04	7.28×10^{-3}	3	2.5×10^{-2}
3100568	5115	4.5	15.76	11.7	3.95×10^{-5}	1	8.2×10^{-3}
3118883	5195	4.5	14.96	8.72	7.13×10^{-3}	4	3.3×10^{-2}
3217974	5221	4.6	15.64	7.29	3.25×10^{-4}	1	8.2×10^{-3}
3239219	5765	4.6	14.51	1.76	9.33×10^{-4}	1	8.2×10^{-3}
3425756	5417	4.6	15.90	23.1	1.16×10^{-3}	7	5.7×10^{-2}
3557532	5221	4.6	14.93	2.04	5.52×10^{-3}	7	5.7×10^{-2}
3626094	5835	4.3	11.43	0.724	4.86×10^{-4}	3	2.3×10^{-2}
3749062	5536	4.4	16.06	0.884	4.79×10^{-5}	1	4.7×10^{-3}
3852071	5484	4.5	16.43	3.70	5.42×10^{-3}	1	1.1×10^{-2}
3869649	5337	4.5	14.87	1.92	1.29×10^{-2}	1	8.2×10^{-3}
3939069	5153	4.5	14.71	17.3	8.97×10^{-4}	1	8.2×10^{-3}
4045215	5229	4.5	14.19	8.21	8.20×10^{-5}	1	7.5×10^{-3}
4138557	5675	4.5	12.37	0.986	1.98×10^{-4}	2	1.5×10^{-2}
4245449	5761	4.0	12.95	2.06	3.04×10^{-3}	1	7.5×10^{-3}
4449749	5198	4.6	15.30	5.68	4.01×10^{-3}	1	8.2×10^{-3}
4742436	5628	4.2	10.99	2.30	6.02×10^{-4}	14	1.1×10^{-1}
4749912	5554	4.3	14.61	4.70	4.07×10^{-3}	2	1.6×10^{-2}
4750938	5804	4.3	13.30	2.06	1.43×10^{-3}	1	7.5×10^{-3}
4830001	5217	4.4	13.98	0.996	6.24×10^{-3}	1	1.1×10^{-2}
4831454	5298	4.6	11.17	5.19	1.51×10^{-3}	3	2.3×10^{-2}
5179841	5252	4.2	13.68	5.09	6.87×10^{-4}	1	7.5×10^{-3}
5350447	5575	4.4	15.73	4.43	7.29×10^{-5}	3	2.5×10^{-2}
5427641	5183	4.4	15.16	3.39	8.83×10^{-3}	1	8.2×10^{-3}
5445334	5137	4.7	13.36	9.44	7.57×10^{-4}	1	8.2×10^{-3}
5474356	5364	4.5	15.47	0.624	3.15×10^{-4}	1	8.2×10^{-3}
5522535	5732	4.3	14.25	6.03	1.94×10^{-5}	1	8.2×10^{-3}
5528061	5424	4.6	15.48	3.82	4.07×10^{-3}	6	4.9×10^{-2}
5529084	5232	4.6	16.06	9.63	4.66×10^{-3}	1	8.2×10^{-3}
5616432	5672	4.4	14.29	4.22	3.65×10^{-3}	1	8.2×10^{-3}
5729515	5529	4.2	13.94	3.89	2.45×10^{-3}	1	8.2×10^{-3}
5896387	5560	4.4	13.73	5.51	1.29×10^{-3}	1	7.5×10^{-3}
6032920	5611	4.6	13.93	3.19	4.80×10^{-4}	5	4.1×10^{-2}
6034120	5407	4.7	15.43	5.68	4.05×10^{-3}	10	8.2×10^{-2}
6127565	5305	4.1	14.18	2.56	3.66×10^{-4}	4	3.0×10^{-2}

[1] These data are taken from the Kepler Input Catalog. [2] The period of the largest amplitude component of the brightness variations in unit of day. [3] The normalized amplitude of the dominant period. [4] The number of detected flares.

Table S1: List of G-type main sequence stars showing superflares (cont.)

KPID	$T_{\rm eff}$[1]	$\log g$[1]	g mag.[1]	Period[2]	Amplitude[3]	N[4]	Flare rate (d^{-1})
6196021	5334	4.2	15.36	2.08	1.57×10^{-4}	5	4.1×10^{-2}
6277018	5725	4.5	15.53	1.77	2.15×10^{-4}	1	8.2×10^{-3}
6292596	5132	4.5	15.38	4.61	4.02×10^{-4}	1	8.2×10^{-3}
6347656	5414	4.4	15.43	8.29	1.19×10^{-4}	1	8.2×10^{-3}
6503434	5714	4.3	13.06	3.89	2.30×10^{-4}	2	1.5×10^{-2}
6507334	5996	4.4	15.25	1.81	2.43×10^{-3}	1	8.2×10^{-3}
6633602	5249	4.7	15.34	4.43	1.52×10^{-5}	1	8.2×10^{-3}
6691930	5348	4.5	16.11	12.8	1.09×10^{-2}	7	5.7×10^{-2}
6697041	5204	4.4	14.94	15.7	6.57×10^{-3}	7	5.7×10^{-2}
6836589	5409	4.2	14.63	0.732	8.78×10^{-3}	1	8.2×10^{-3}
6848592	5378	4.4	14.54	1.65	1.75×10^{-3}	1	8.2×10^{-3}
6865416	5222	4.4	14.28	3.29	1.03×10^{-2}	2	1.6×10^{-2}
6865484	5688	4.4	14.24	11.0	1.33×10^{-3}	3	2.5×10^{-2}
7093547	5101	4.3	14.39	6.66	1.06×10^{-4}	1	8.2×10^{-3}
7133671	5657	4.4	15.98	3.25	1.84×10^{-5}	1	4.7×10^{-3}
7174505	5220	4.4	15.13	3.78	7.28×10^{-3}	14	1.1×10^{-1}
7256548	5306	4.9	16.04	6.15	3.17×10^{-3}	1	8.2×10^{-3}
7264976	5184	4.1	12.54	12.7	9.84×10^{-3}	8	6.0×10^{-2}
7287601	5461	4.6	15.12	16.2	1.66×10^{-3}	1	8.2×10^{-3}
7368914	5984	4.5	16.14	1.98	1.17×10^{-3}	1	5.6×10^{-3}
7532880	5562	4.4	13.52	2.14	4.32×10^{-3}	3	2.3×10^{-2}
7667812	5830	4.3	13.11	1.79	5.72×10^{-4}	2	1.5×10^{-2}
7902097	5626	4.6	12.70	3.89	2.28×10^{-3}	1	7.5×10^{-3}
8009474	5307	4.6	15.92	15.4	8.67×10^{-3}	1	8.2×10^{-3}
8074287	5488	4.4	14.78	2.78	1.91×10^{-3}	2	1.6×10^{-2}
8076634	5215	4.7	15.75	6.28	2.58×10^{-3}	1	8.2×10^{-3}
8091757	5871	4.6	13.42	2.04	3.99×10^{-4}	3	2.3×10^{-2}
8143783	5625	4.6	16.21	0.739	4.60×10^{-3}	1	1.1×10^{-2}
8162830	5770	4.6	15.51	2.56	5.54×10^{-3}	5	4.1×10^{-2}
8212826	5811	4.2	14.38	1.03	2.19×10^{-5}	1	8.2×10^{-3}
8226464	5754	4.1	11.86	3.10	3.18×10^{-3}	6	2.7×10^{-2}
8302223	5683	4.5	14.89	9.63	7.73×10^{-3}	1	8.2×10^{-3}
8359398	5123	4.7	14.68	12.8	2.86×10^{-3}	1	8.2×10^{-3}
8479655	5126	4.6	13.31	19.3	1.18×10^{-2}	6	4.5×10^{-2}
8480296	5741	4.5	16.20	0.996	1.01×10^{-3}	1	5.6×10^{-3}
8482482	5521	4.5	15.86	4.61	5.49×10^{-3}	3	2.5×10^{-2}
8491470	5340	4.9	14.86	5.41	2.65×10^{-3}	4	3.3×10^{-2}

[1] These data are taken from the Kepler Input Catalog. [2] The period of the largest amplitude component of the brightness variations in unit of day. [3] The normalized amplitude of the dominant period. [4] The number of detected flares.

Table S1: List of G-type main sequence stars showing superflares (cont.)

KPID	$T_{\rm eff}$[1]	$\log g$[1]	g mag.[1]	Period[2]	Amplitude[3]	N[4]	Flare rate (d^{-1})
8547383	5376	4.5	14.75	14.5	1.08×10^{-3}	11	9.0×10^{-2}
8604805	5294	4.5	15.15	2.86	7.72×10^{-3}	1	8.2×10^{-3}
8613466	5535	4.5	15.27	2.41	2.44×10^{-3}	3	2.5×10^{-2}
8621739	5940	4.4	13.92	0.920	1.50×10^{-3}	1	7.5×10^{-3}
8802001	5815	4.5	14.19	1.85	3.46×10^{-4}	1	8.2×10^{-3}
8848528	5586	4.1	13.93	1.29	2.07×10^{-3}	1	7.5×10^{-3}
8935644	5855	4.3	15.76	3.67	6.72×10^{-4}	2	1.6×10^{-2}
9146690	5216	4.5	15.71	0.710	4.46×10^{-4}	3	2.5×10^{-2}
9149986	5319	4.4	14.85	1.42	1.19×10^{-2}	1	8.2×10^{-3}
9150539	5409	4.5	15.70	3.25	1.00×10^{-2}	7	5.7×10^{-2}
9410906	5659	4.4	15.13	0.121	3.01×10^{-4}	2	1.6×10^{-2}
9412514	5958	4.2	11.73	1.85	3.71×10^{-5}	1	7.5×10^{-3}
9459362	5357	4.6	14.61	12.5	1.64×10^{-3}	5	4.1×10^{-2}
9583493	5445	4.5	13.12	5.30	4.47×10^{-3}	1	7.5×10^{-3}
9630984	5590	4.5	16.25	16.6	1.02×10^{-3}	1	5.6×10^{-3}
9652680	5618	4.8	11.61	1.41	9.06×10^{-3}	1	4.5×10^{-3}
9653110	5223	4.4	13.40	3.10	9.51×10^{-3}	1	7.5×10^{-3}
9655134	5229	4.5	14.20	7.58	1.85×10^{-3}	5	2.4×10^{-2}
9764192	5551	4.6	13.40	3.52	5.21×10^{-3}	1	7.5×10^{-3}
9764489	5447	4.7	14.65	10.6	4.58×10^{-3}	1	8.2×10^{-3}
9786953	5168	4.5	14.09	7.36	4.28×10^{-3}	1	7.5×10^{-3}
9838078	5164	5.0	15.38	0.612	3.33×10^{-3}	1	8.2×10^{-3}
9897464	5538	4.4	15.55	3.45	3.54×10^{-3}	2	1.6×10^{-2}
9934388	5578	4.4	16.09	0.920	6.63×10^{-3}	3	1.7×10^{-2}
10000785	5145	4.5	16.36	1.25	8.77×10^{-3}	1	1.1×10^{-2}
10120296	5490	4.4	13.33	3.85	7.95×10^{-3}	4	3.3×10^{-2}
10220756	5753	4.2	13.83	4.94	5.30×10^{-3}	3	2.3×10^{-2}
10287991	5336	4.8	16.54	0.911	1.40×10^{-2}	1	8.2×10^{-3}
10398088	5368	4.4	13.44	5.63	1.17×10^{-4}	1	7.5×10^{-3}
10422252	5118	4.2	14.28	5.41	3.59×10^{-3}	11	9.0×10^{-2}
10453475	5202	4.5	14.76	15.2	6.60×10^{-3}	2	1.6×10^{-2}
10471412	5771	4.1	13.89	17.1	7.12×10^{-4}	1	7.5×10^{-3}
10489814	5436	4.7	15.20	3.16	5.54×10^{-3}	2	1.6×10^{-2}
10524994	5747	4.5	15.80	11.7	1.94×10^{-3}	1	8.2×10^{-3}
10528093	5143	4.5	14.13	12.8	5.42×10^{-3}	7	5.3×10^{-2}
10583379	5743	4.4	14.64	3.70	3.49×10^{-3}	1	8.2×10^{-3}
10593098	5129	4.2	14.43	7.58	6.25×10^{-3}	1	8.2×10^{-3}

[1] These data are taken from the Kepler Input Catalog. [2] The period of the largest amplitude component of the brightness variations in unit of day. [3] The normalized amplitude of the dominant period. [4] The number of detected flares.

Table S1: List of G-type main sequence stars showing superflares (cont.)

KPID	$T_{\rm eff}^{1}$	$\log g^{1}$	g mag.[1]	Period[2]	Amplitude[3]	N[4]	Flare rate (d^{-1})
10646889	5483	4.4	14.10	5.09	2.89×10^{-3}	2	4.5×10^{-2}
10745663	5754	4.6	14.80	3.19	7.01×10^{-3}	2	6.0×10^{-2}
10796663	5336	4.2	13.72	7.29	1.71×10^{-3}	2	1.5×10^{-2}
10809099	5775	4.6	16.16	0.902	2.04×10^{-4}	1	8.2×10^{-3}
10919564	5474	4.6	16.27	0.463	1.62×10^{-4}	1	8.2×10^{-3}
10969515	5186	4.5	15.02	5.35	4.39×10^{-3}	1	8.2×10^{-3}
10992714	5438	4.3	15.58	2.25	5.59×10^{-3}	2	1.6×10^{-2}
11020468	5255	4.7	15.52	5.80	4.14×10^{-3}	2	1.6×10^{-2}
11073910	5381	4.6	12.16	5.57	1.90×10^{-3}	2	1.5×10^{-2}
11091597	5101	4.2	15.74	1.92	1.10×10^{-2}	2	1.6×10^{-2}
11136848	5999	4.6	14.65	5.46	9.07×10^{-4}	1	8.2×10^{-3}
11186775	5948	4.3	14.28	1.77	2.02×10^{-3}	2	1.6×10^{-2}
11235754	5240	4.6	15.81	6.80	3.95×10^{-3}	1	8.2×10^{-3}
11235995	5251	4.5	15.67	5.14	8.59×10^{-3}	2	1.6×10^{-2}
11283805	5218	4.1	14.44	4.17	1.04×10^{-3}	3	2.5×10^{-2}
11285287	5146	4.6	15.32	6.34	2.19×10^{-4}	1	8.2×10^{-3}
11390058	5785	4.3	13.02	11.9	2.81×10^{-4}	2	1.5×10^{-2}
11401109	5732	4.5	14.98	4.70	1.93×10^{-5}	1	8.2×10^{-3}
11454563	5302	4.8	15.36	0.769	2.50×10^{-3}	3	2.5×10^{-2}
11455711	5664	4.7	14.40	13.9	2.90×10^{-3}	2	1.6×10^{-2}
11498907	5964	4.4	13.71	0.866	6.60×10^{-4}	1	7.5×10^{-3}
11610797	5865	4.5	11.88	1.69	2.62×10^{-3}	3	1.8×10^{-2}
11649990	5713	4.3	15.26	2.00	3.61×10^{-4}	2	1.6×10^{-2}
11757490	5790	4.5	14.96	1.25	1.42×10^{-3}	2	1.6×10^{-2}
11764567	5238	4.4	13.79	22.7	2.42×10^{-3}	11	8.3×10^{-2}
11770267	5120	4.8	15.27	1.25	1.38×10^{-3}	1	8.2×10^{-3}
11818232	5556	4.7	15.88	1.01	5.93×10^{-3}	1	8.2×10^{-3}
11924179	5852	4.2	14.14	3.59	4.65×10^{-3}	1	8.2×10^{-3}
11972298	5498	4.4	14.21	15.5	2.31×10^{-3}	2	1.6×10^{-2}
12003808	5126	4.8	16.53	3.67	1.56×10^{-2}	6	4.9×10^{-2}
12006586	5560	4.6	16.36	1.86	2.36×10^{-3}	1	1.1×10^{-2}
12109550	5645	4.1	13.74	4.52	2.41×10^{-3}	1	7.5×10^{-3}
12169825	5400	4.4	14.84	23.3	2.14×10^{-3}	1	8.2×10^{-3}
12266582	5434	4.3	13.46	7.14	2.79×10^{-3}	1	7.5×10^{-3}
12354328	5115	4.4	15.31	0.800	5.55×10^{-3}	3	2.5×10^{-2}
12355626	5757	4.4	14.69	1.04	3.68×10^{-4}	1	8.2×10^{-3}
12401269	5466	4.4	14.81	2.27	1.03×10^{-2}	1	8.2×10^{-3}

[1] These data are taken from the Kepler Input Catalog. [2] The period of the largest amplitude component of the brightness variations in unit of day. [3] The normalized amplitude of the dominant period. [4] The number of detected flares.

Appendix II: Light curves of each superflare

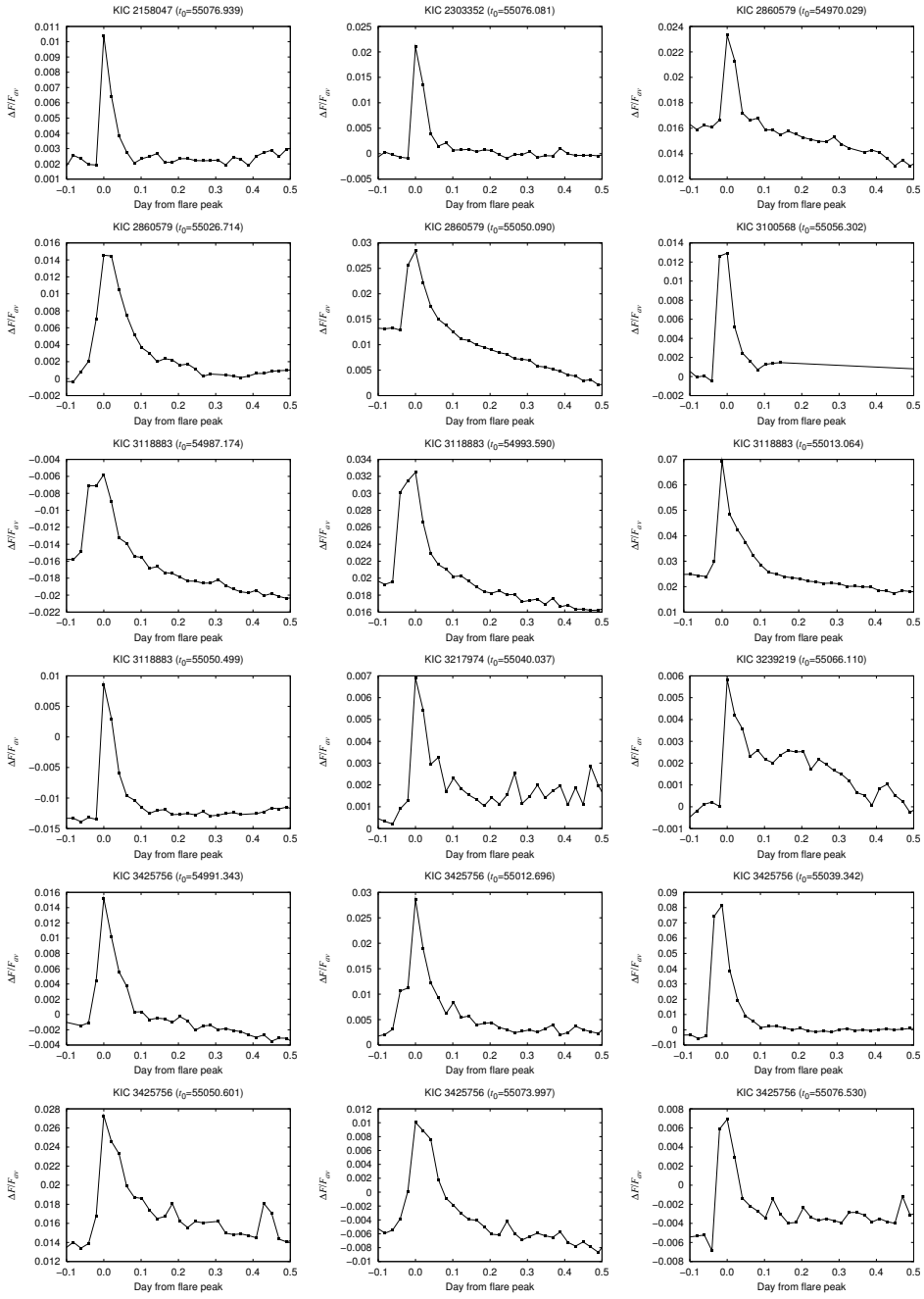

Figure S8: Light curves of each flare. The individual points represent the difference between observed brightness during each cadence and the average brightness during the observation period. The horizontal axis and the vertical axis represent the time from the flare peak (t_0) in unit of day and the normalized brightness difference from the average value.

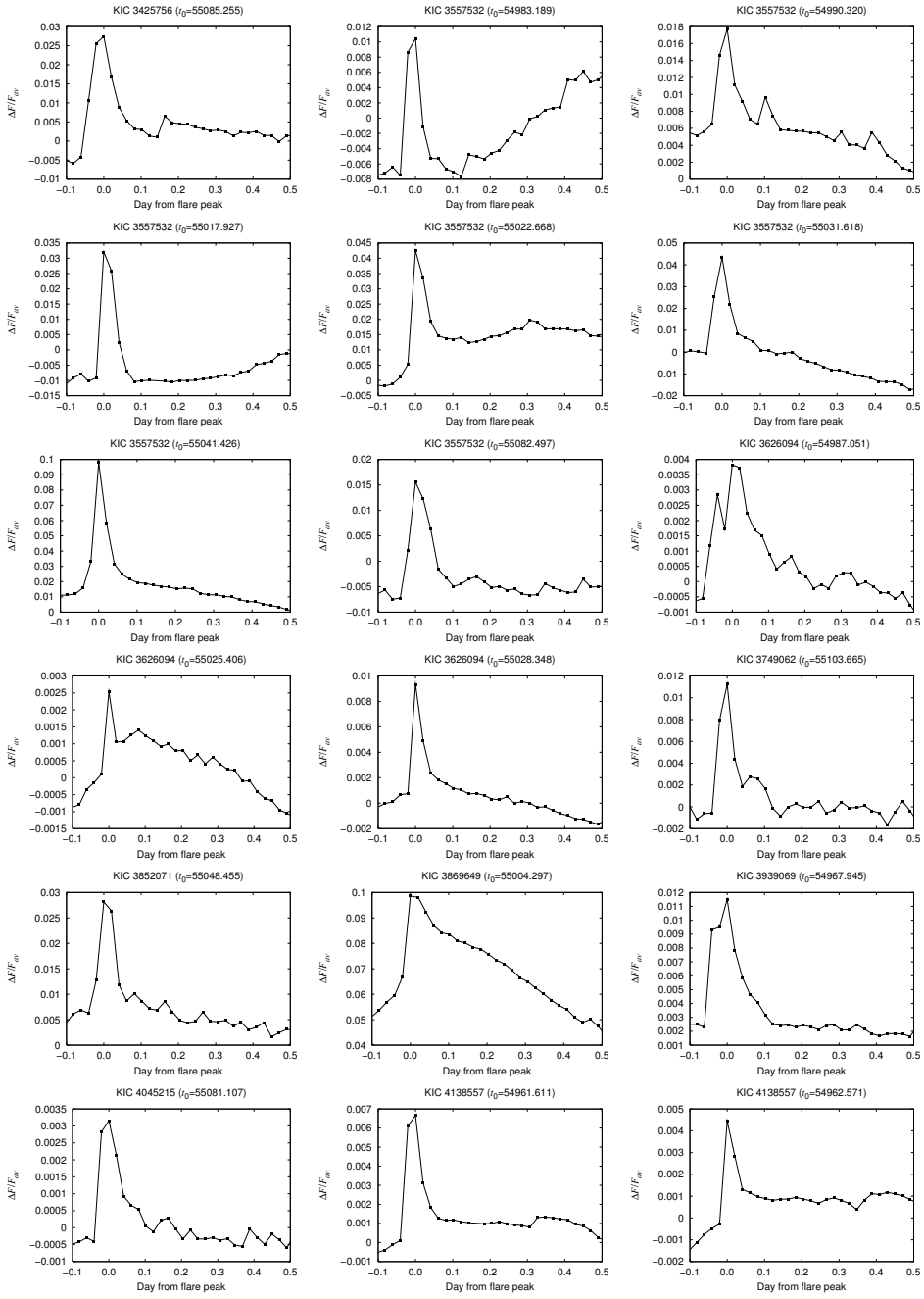

Figure S8: Light curves of each flare (cont.)

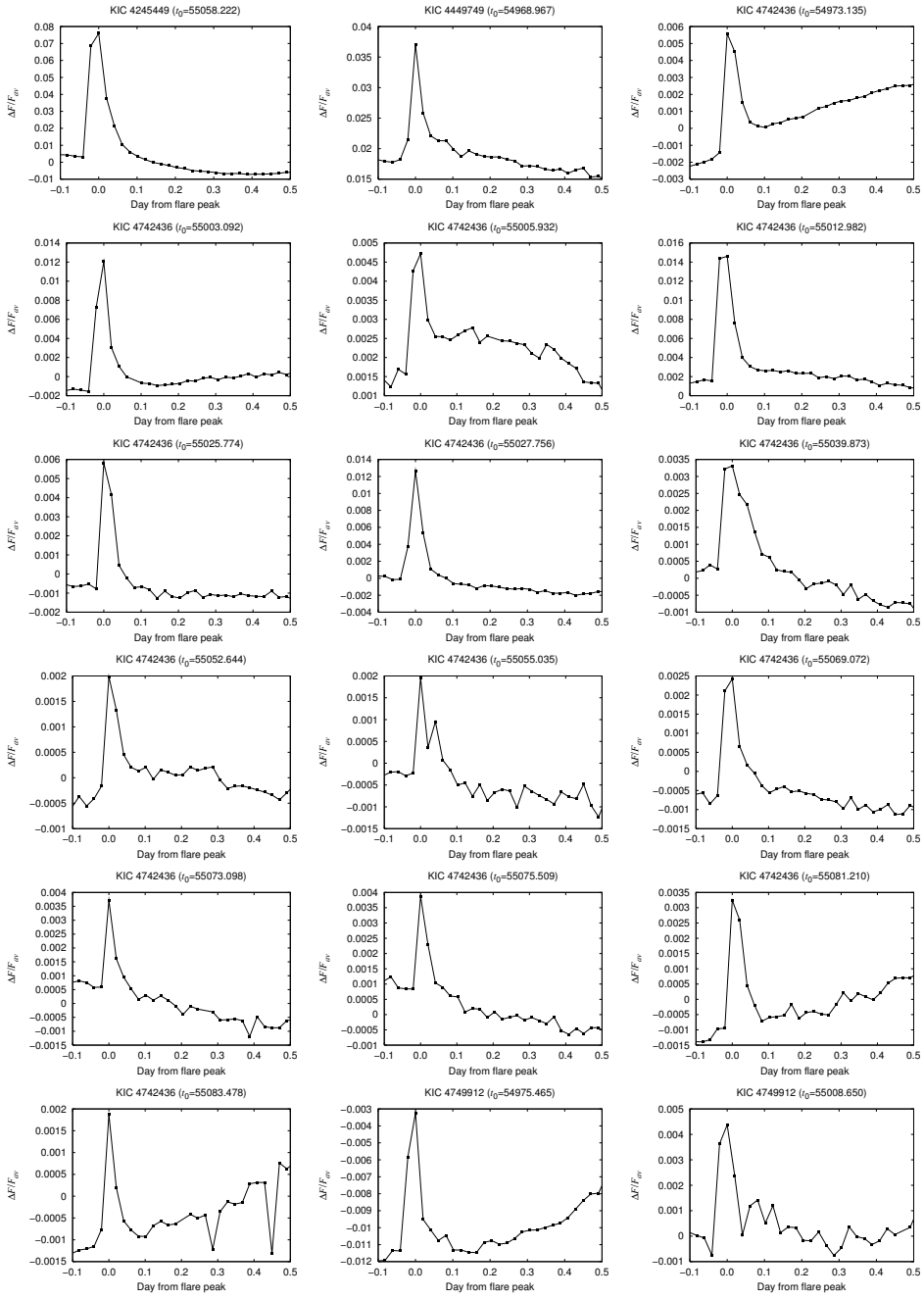

Figure S8: Light curves of each flare (cont.)

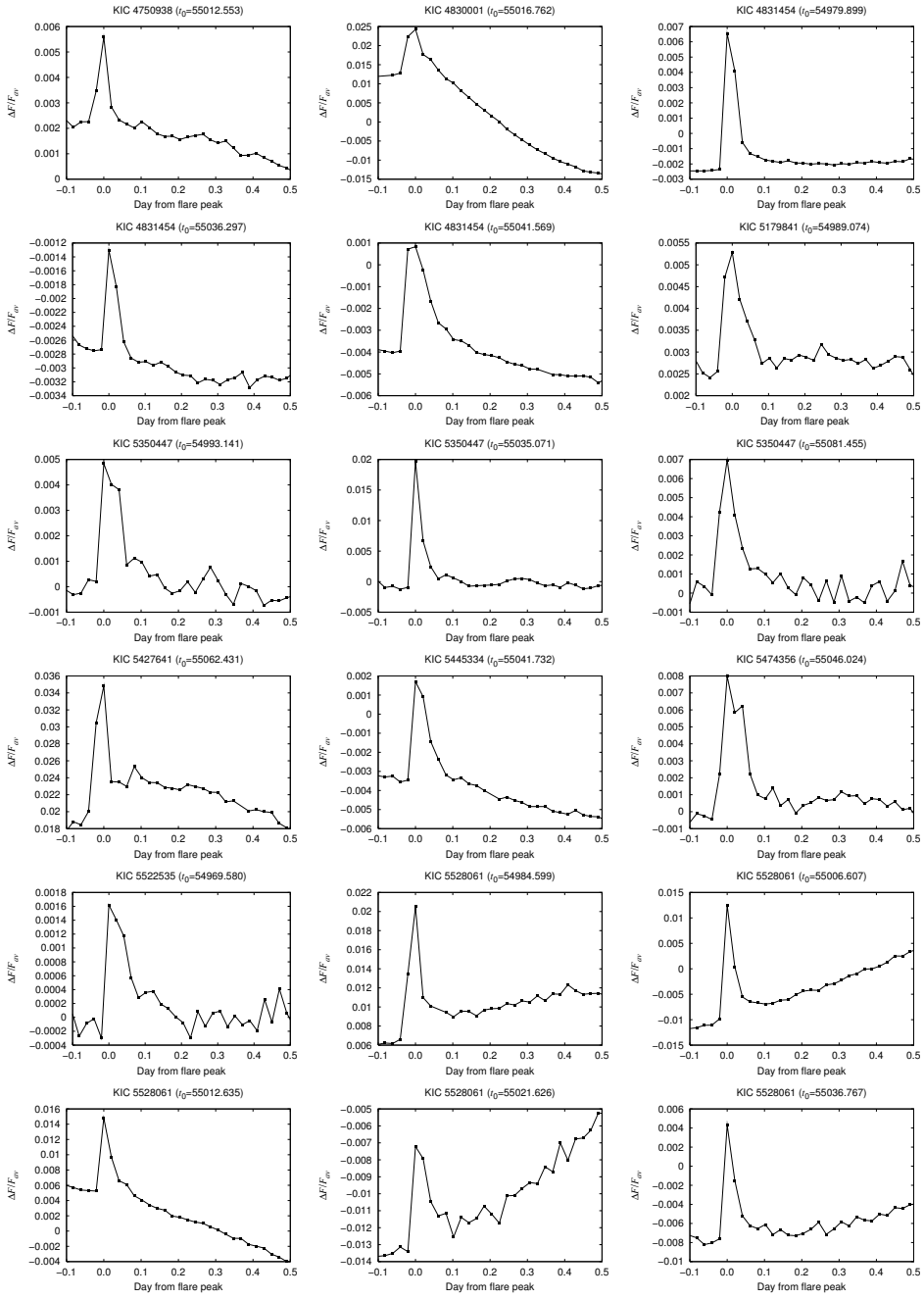

Figure S8: Light curves of each flare (cont.)

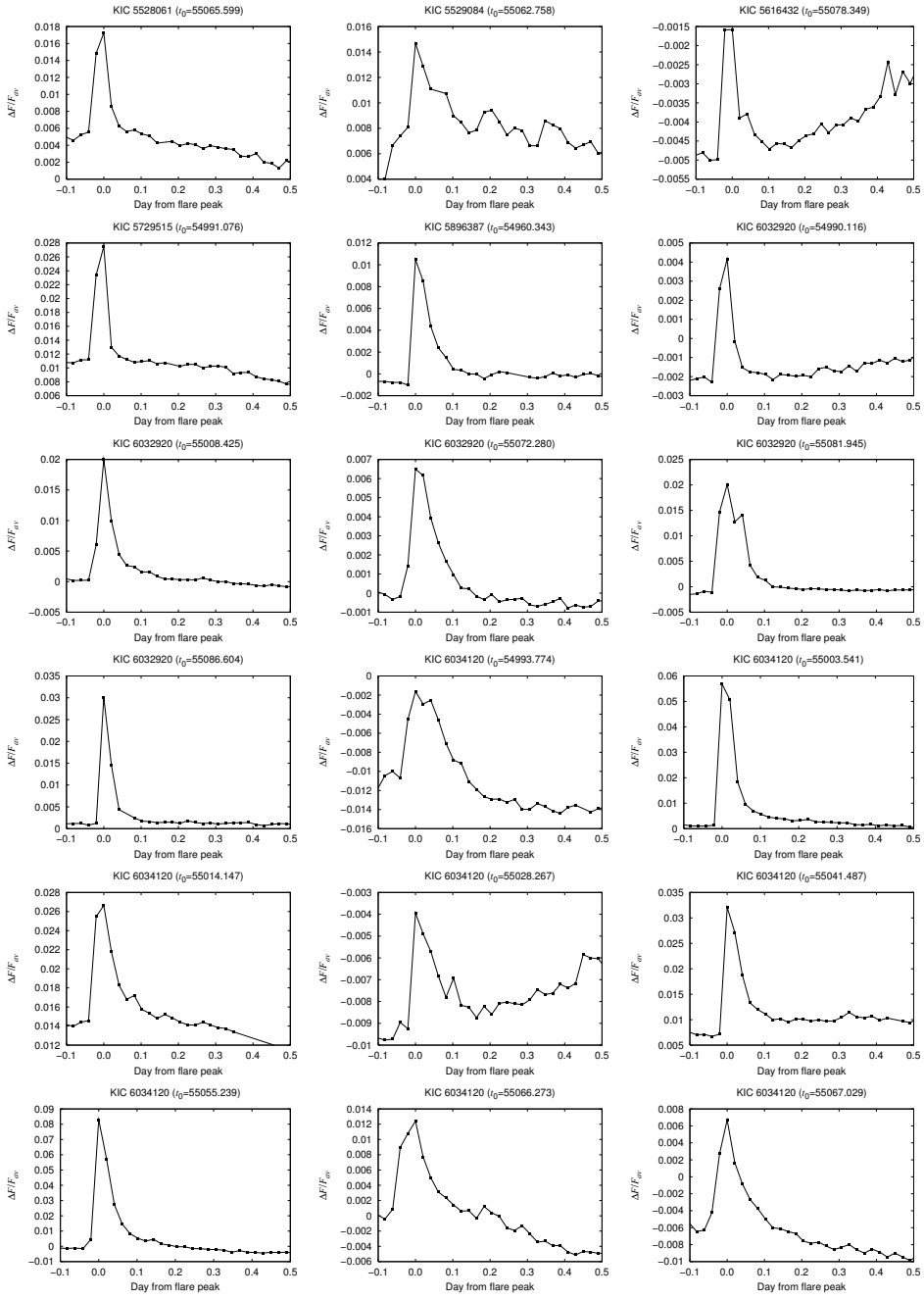

Figure S8: Light curves of each flare (cont.)

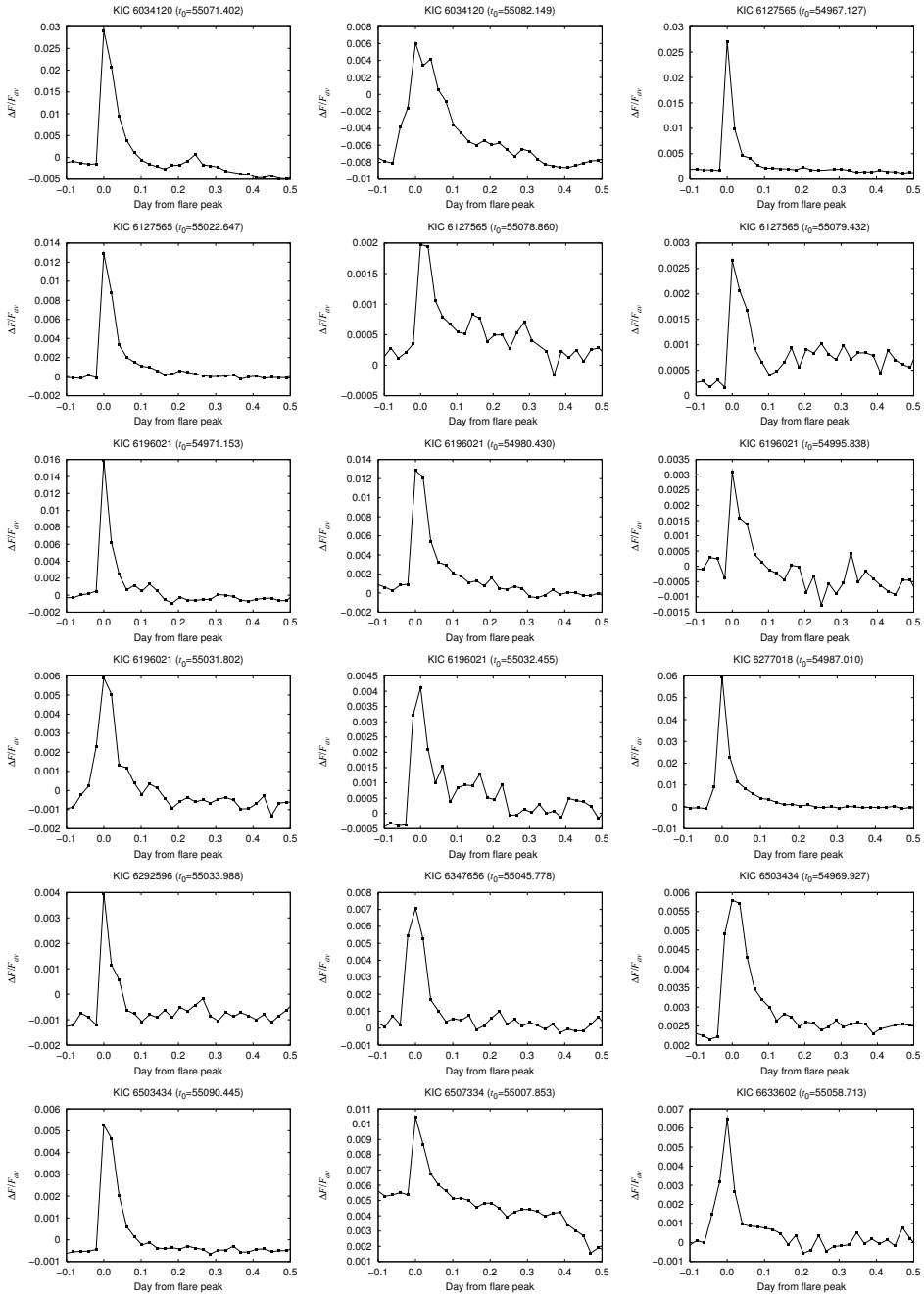

Figure S8: Light curves of each flare (cont.)

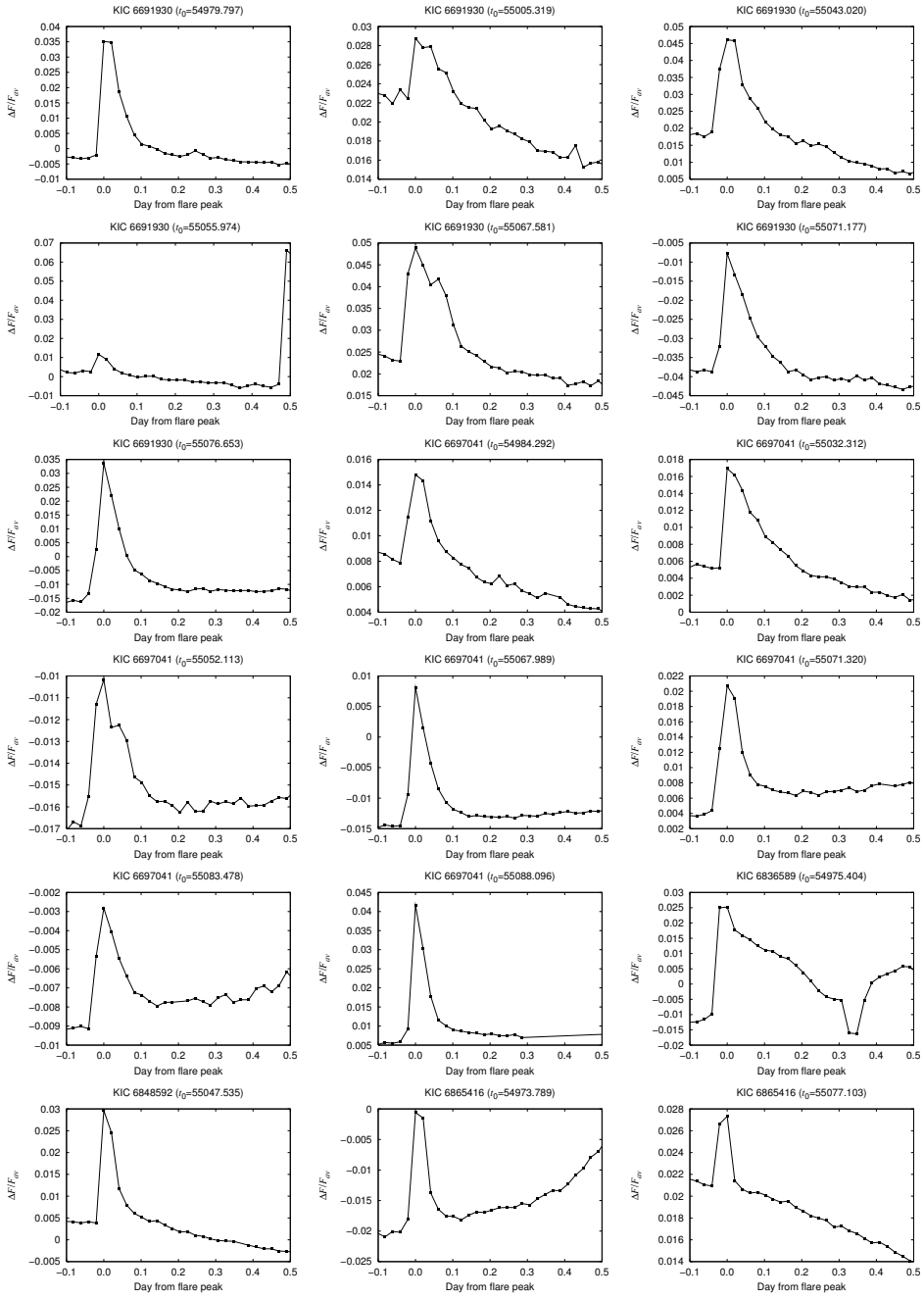

Figure S8: Light curves of each flare (cont.)

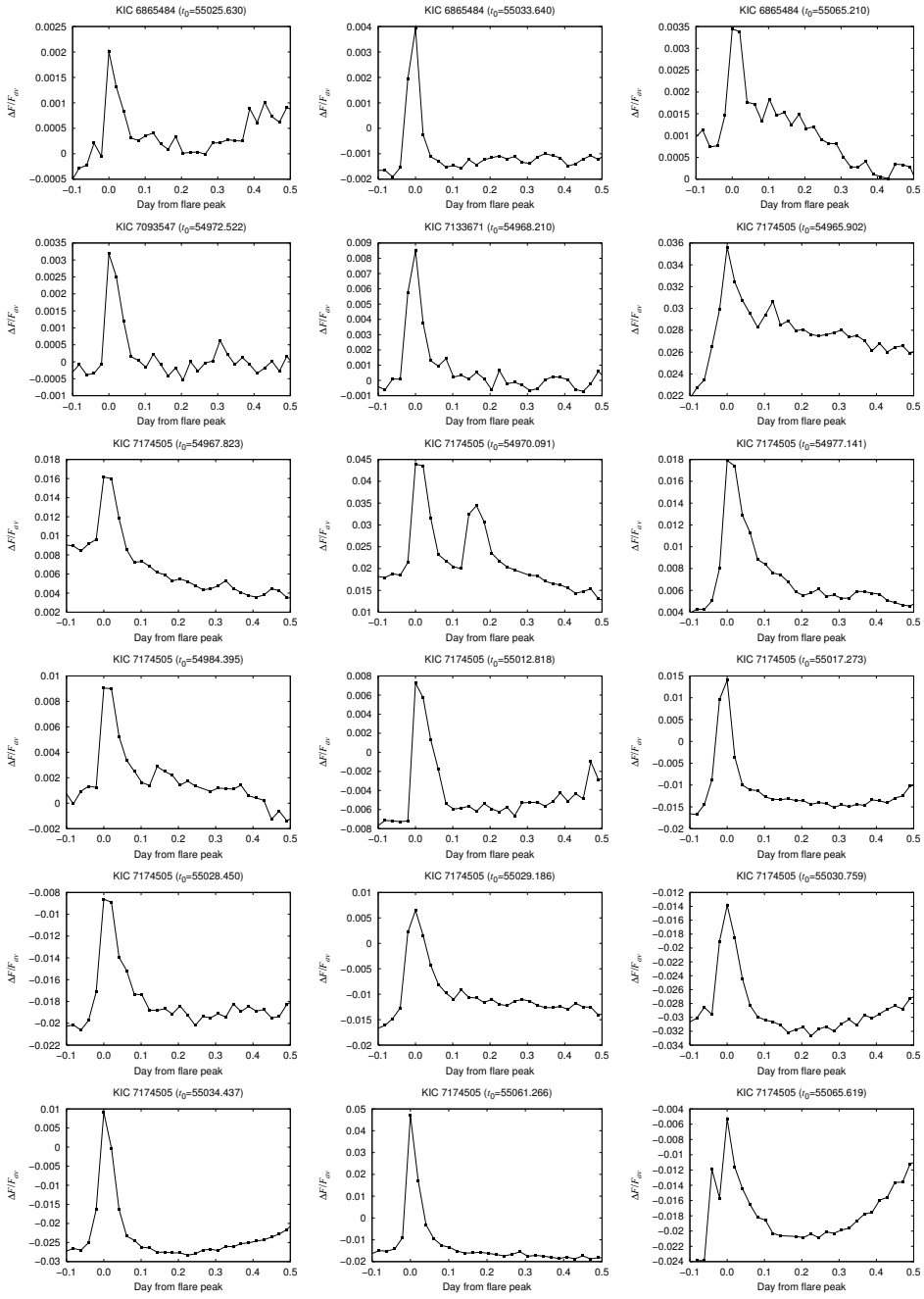

Figure S8: Light curves of each flare (cont.)

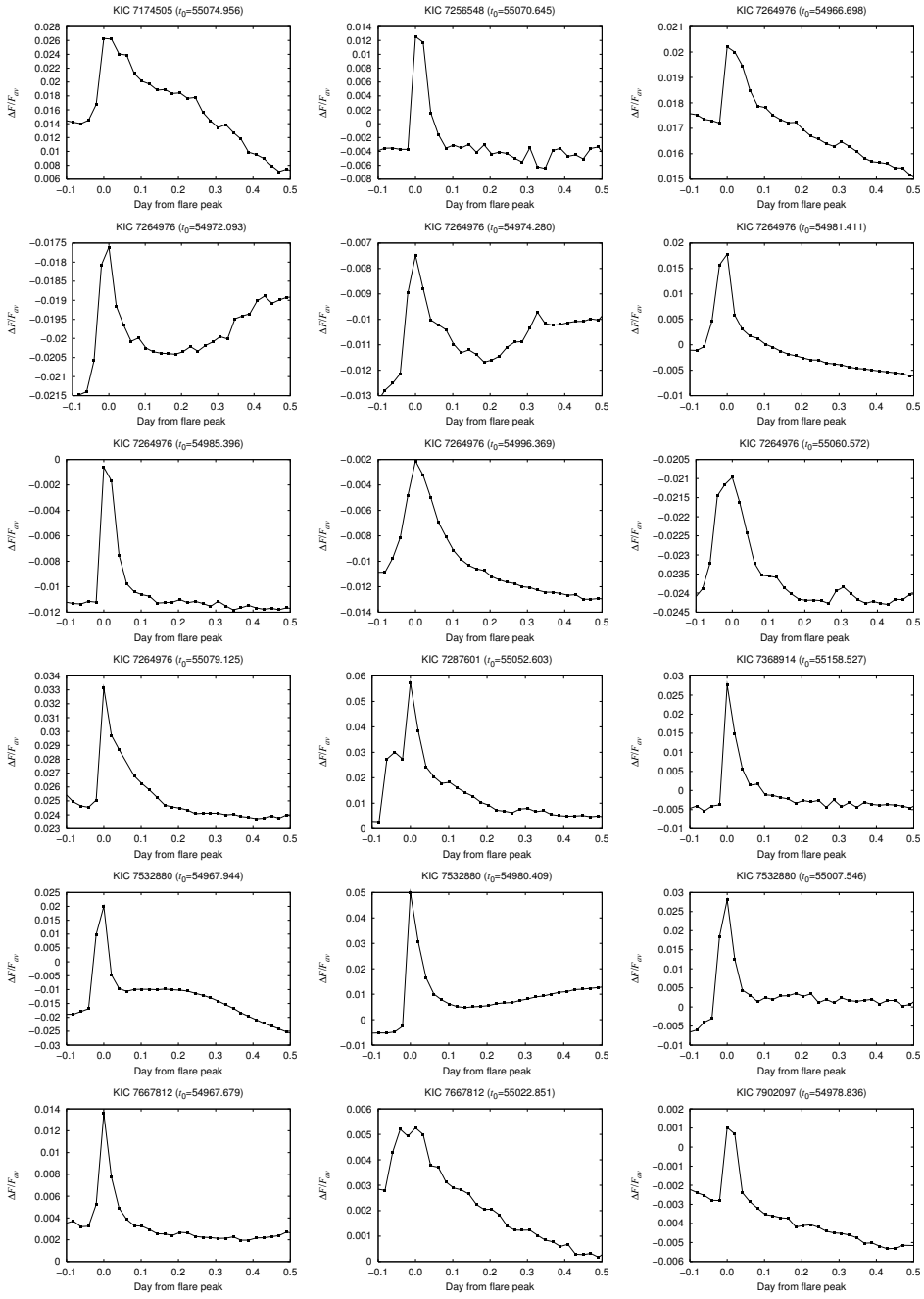

Figure S8: Light curves of each flare (cont.)

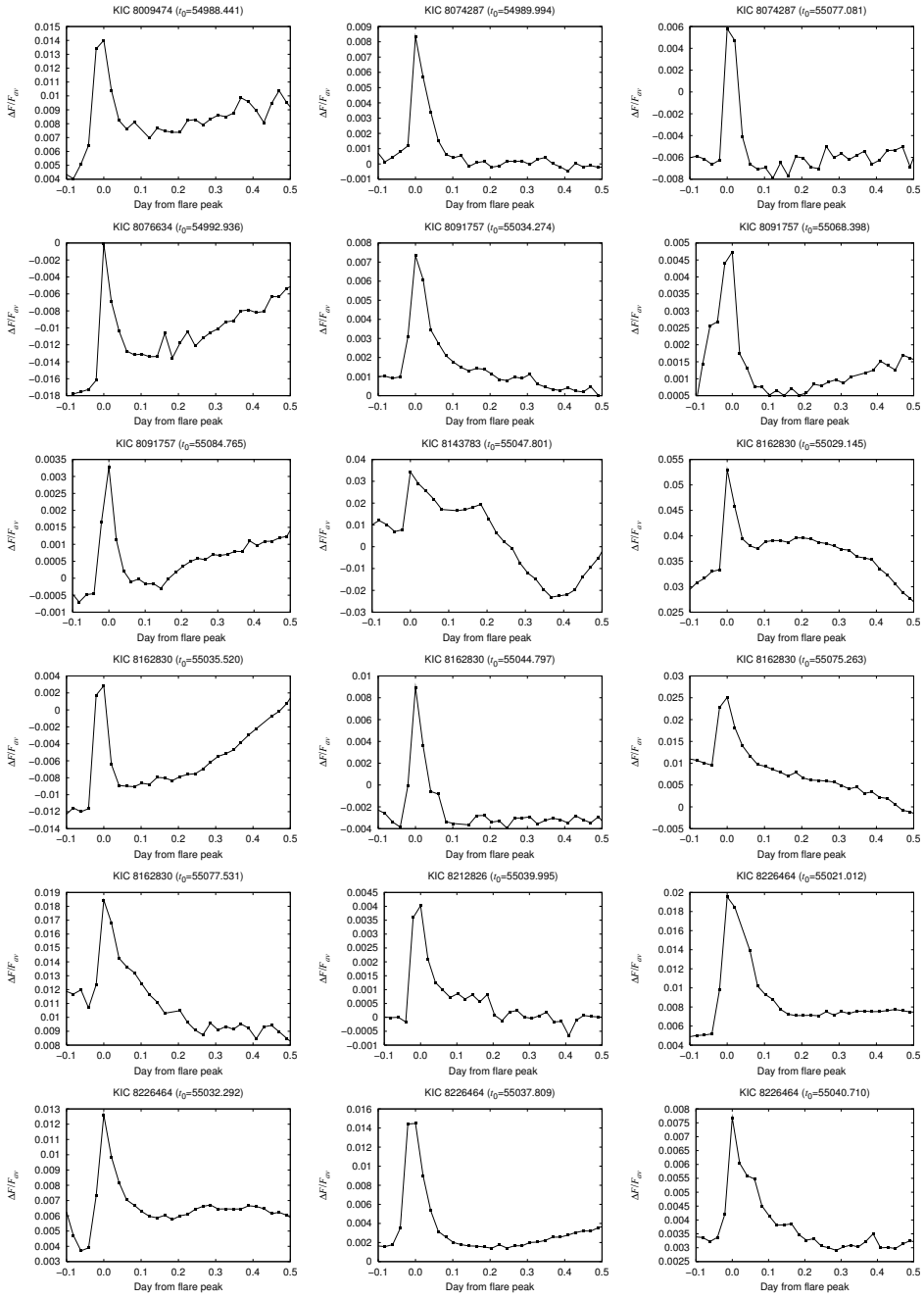

Figure S8: Light curves of each flare (cont.)

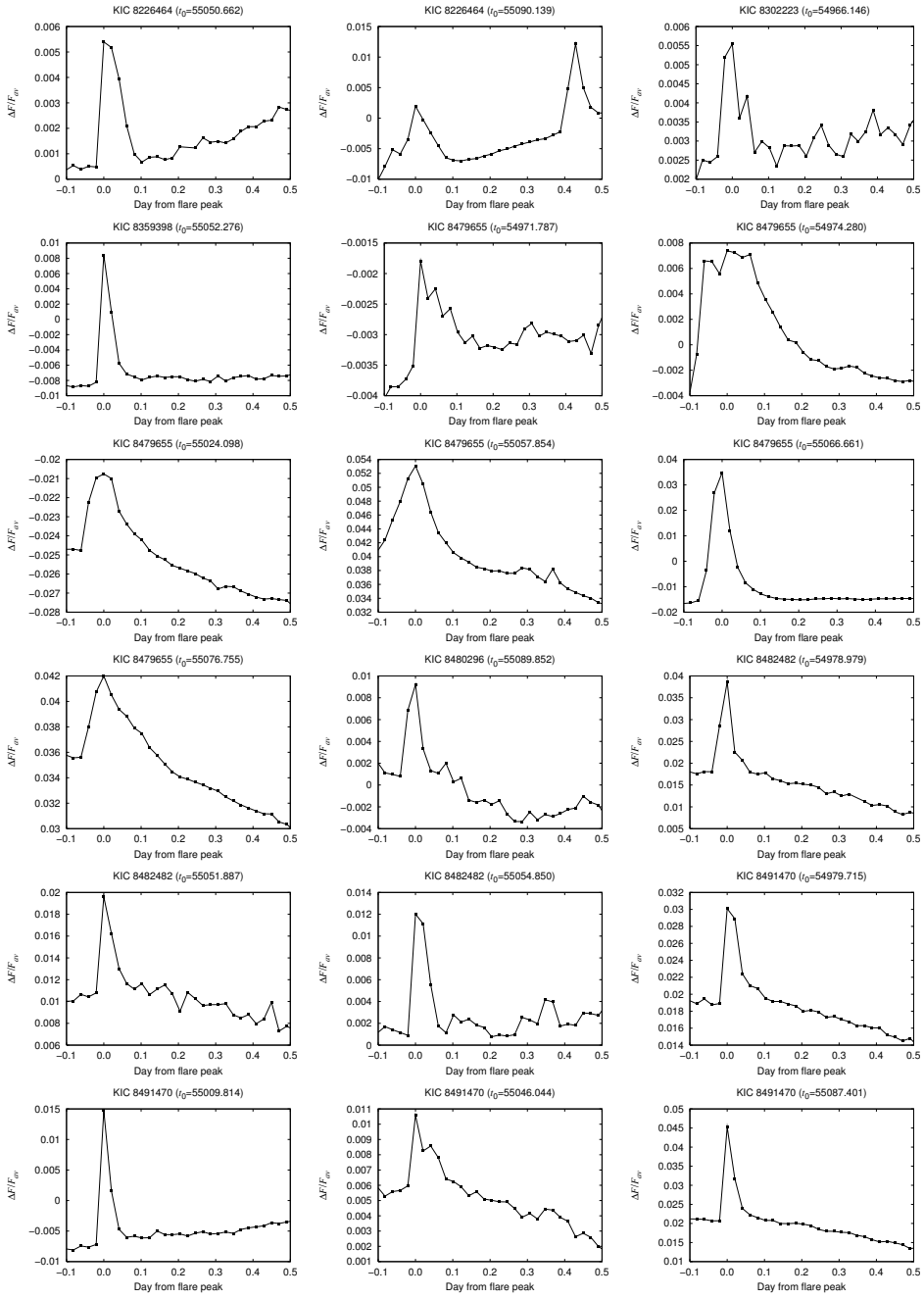

Figure S8: Light curves of each flare (cont.)

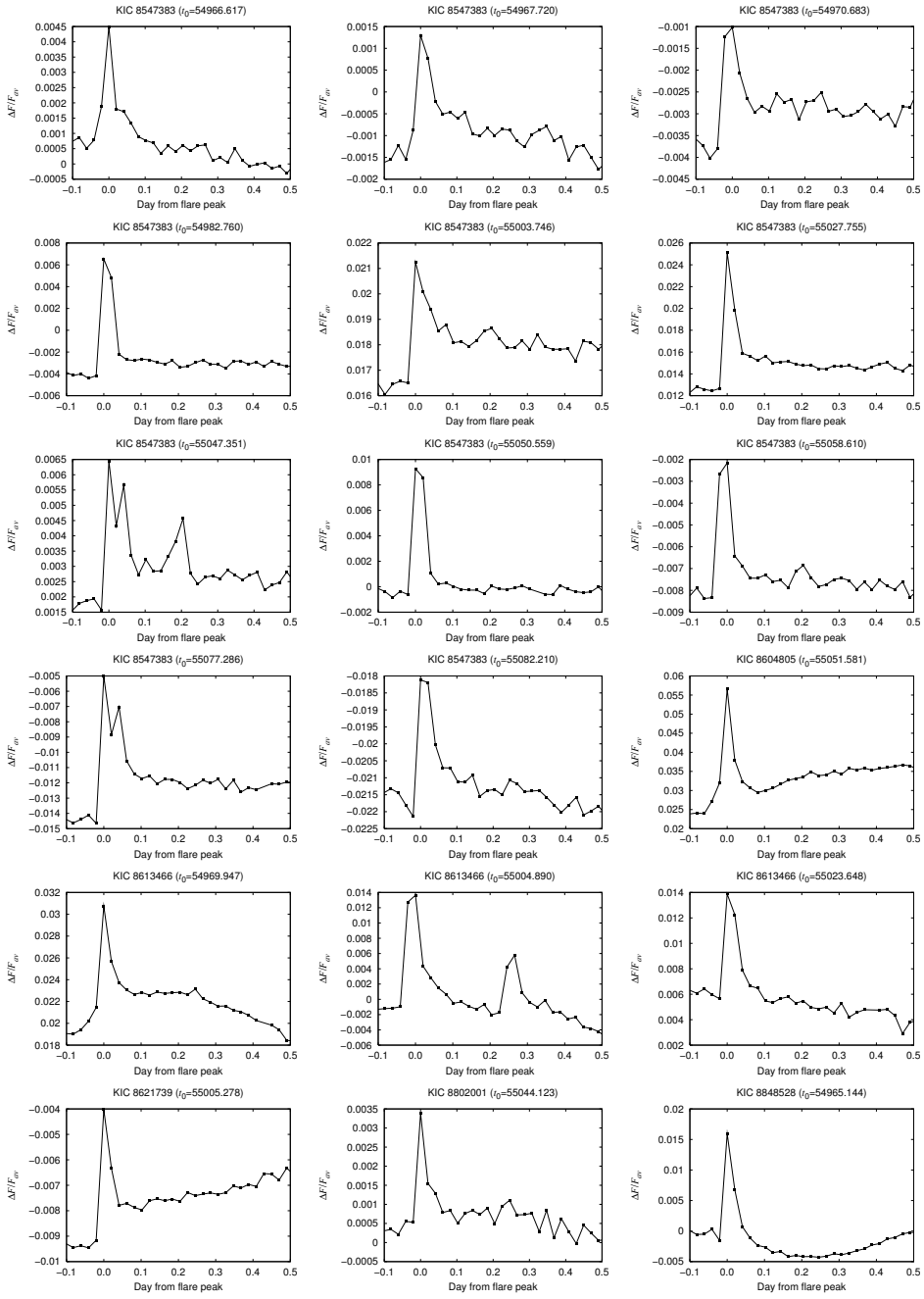

Figure S8: Light curves of each flare (cont.)

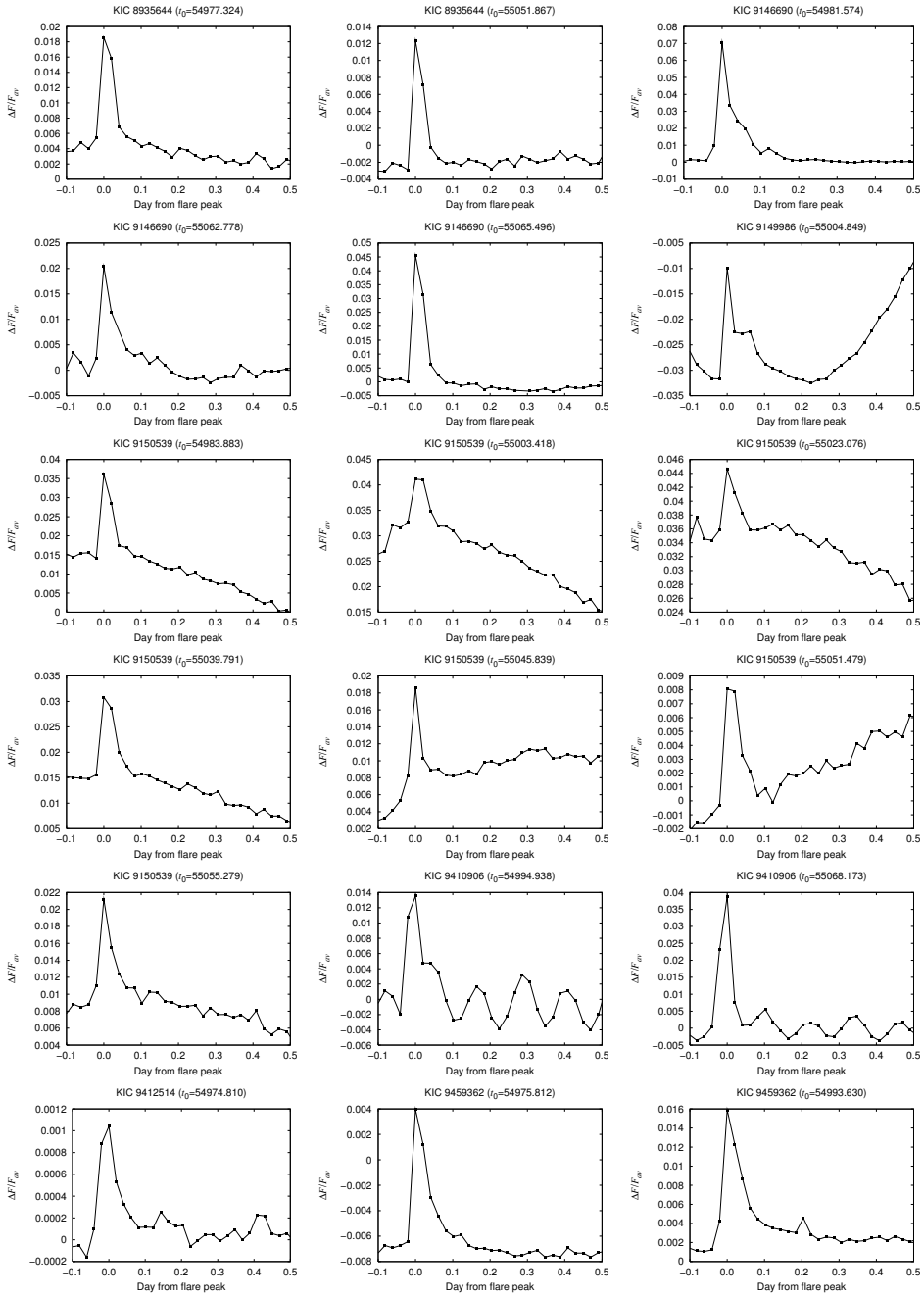

Figure S8: Light curves of each flare (cont.)

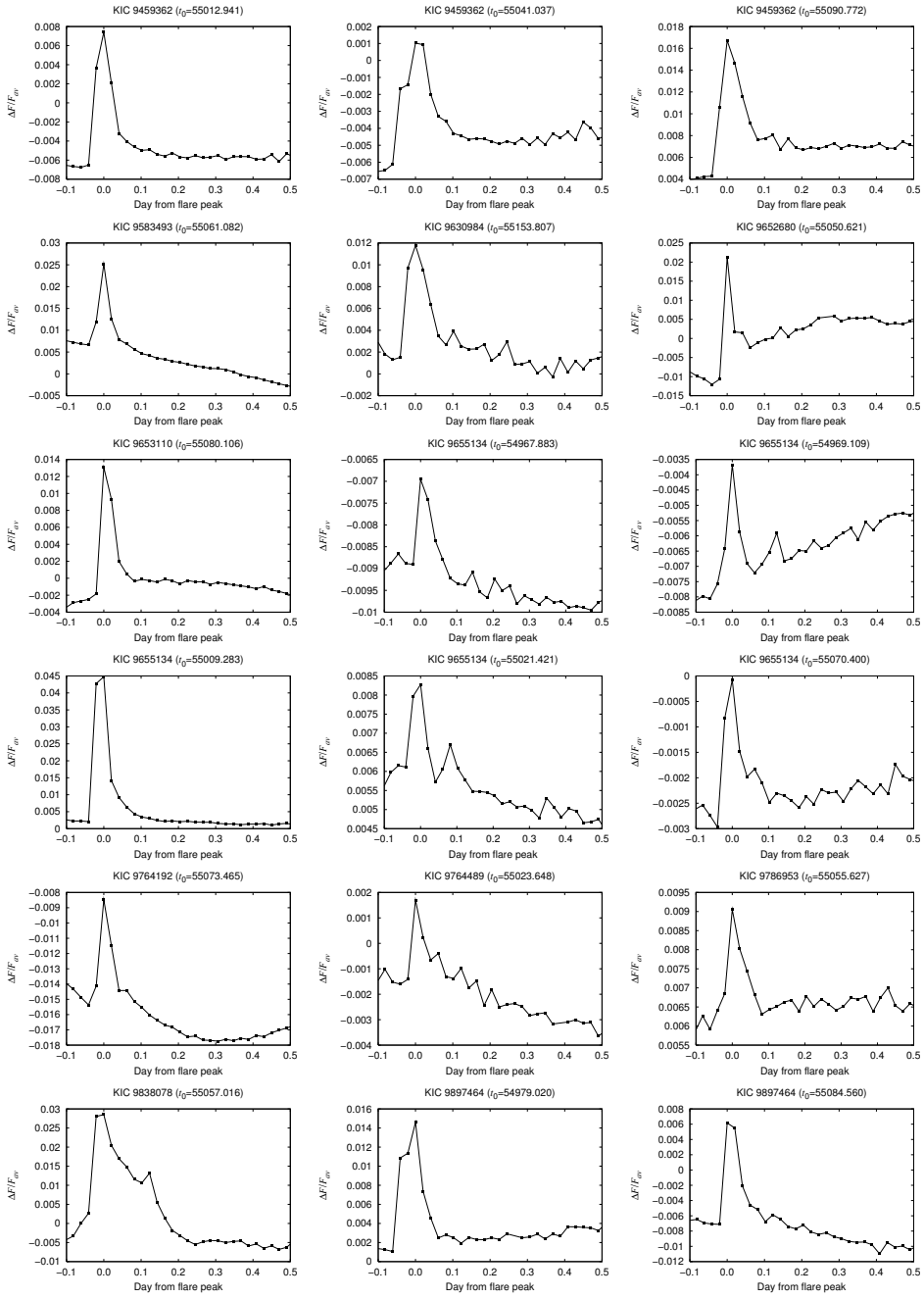

Figure S8: Light curves of each flare (cont.)

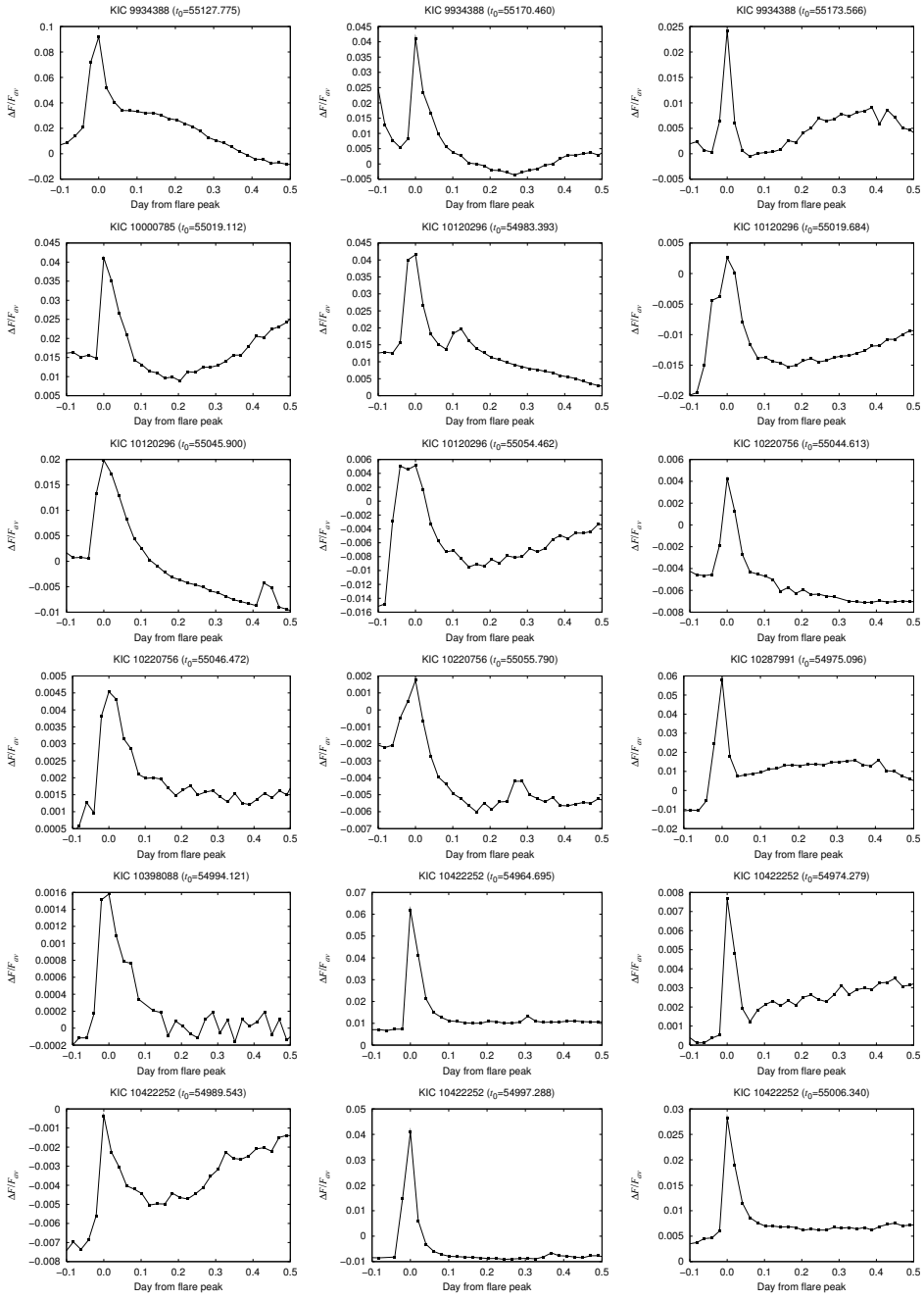

Figure S8: Light curves of each flare (cont.)

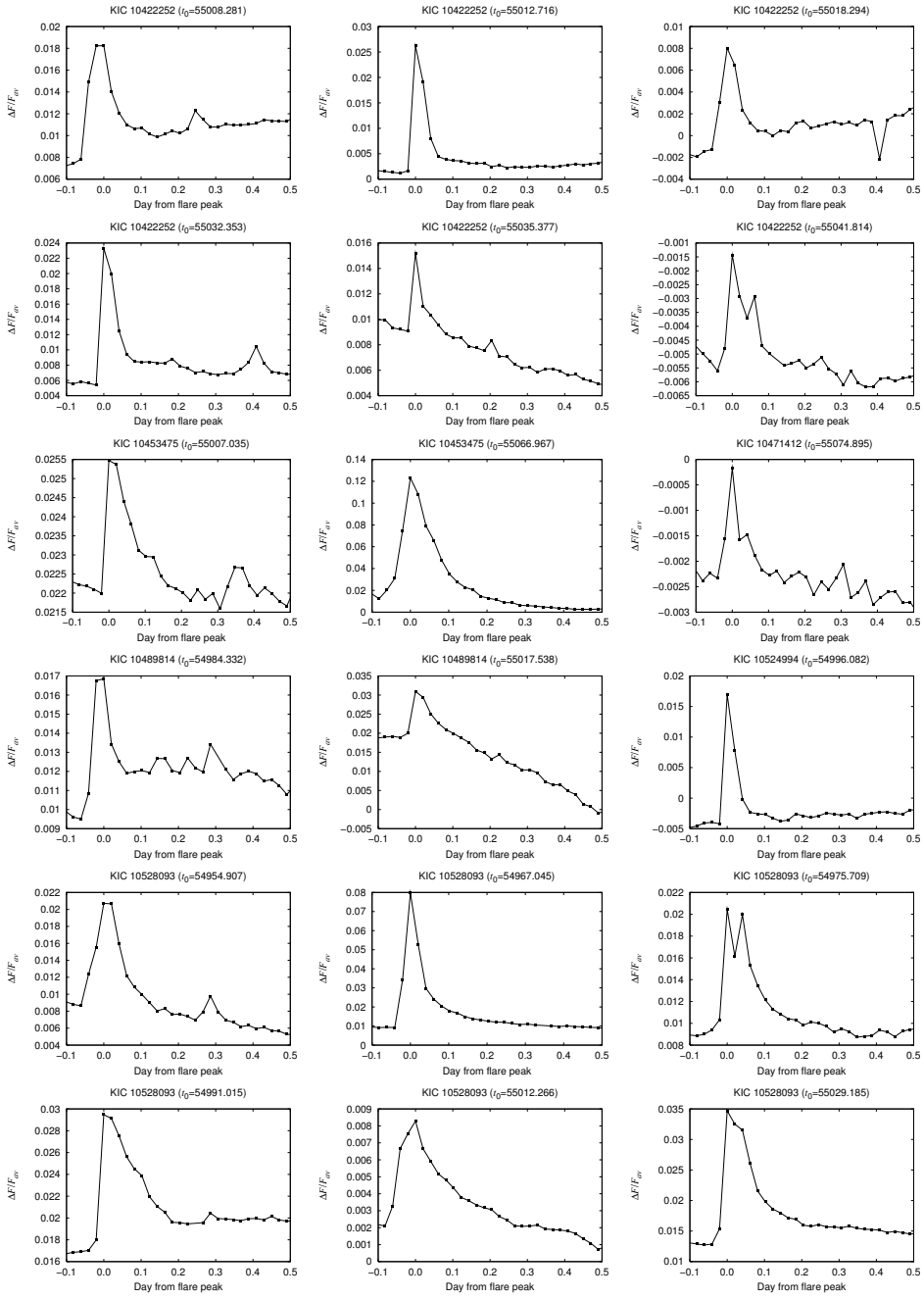

Figure S8: Light curves of each flare (cont.)

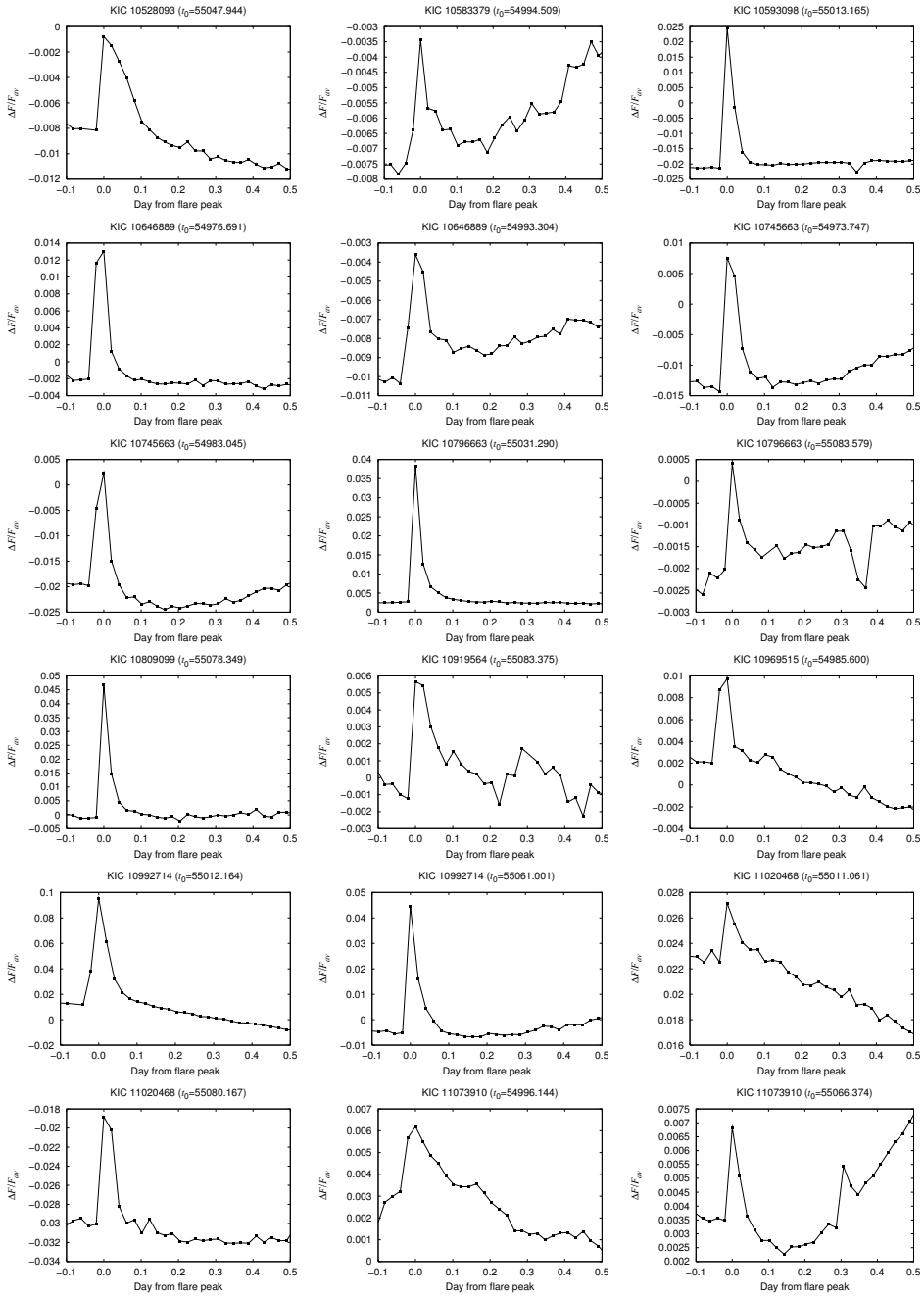

Figure S8: Light curves of each flare (cont.)

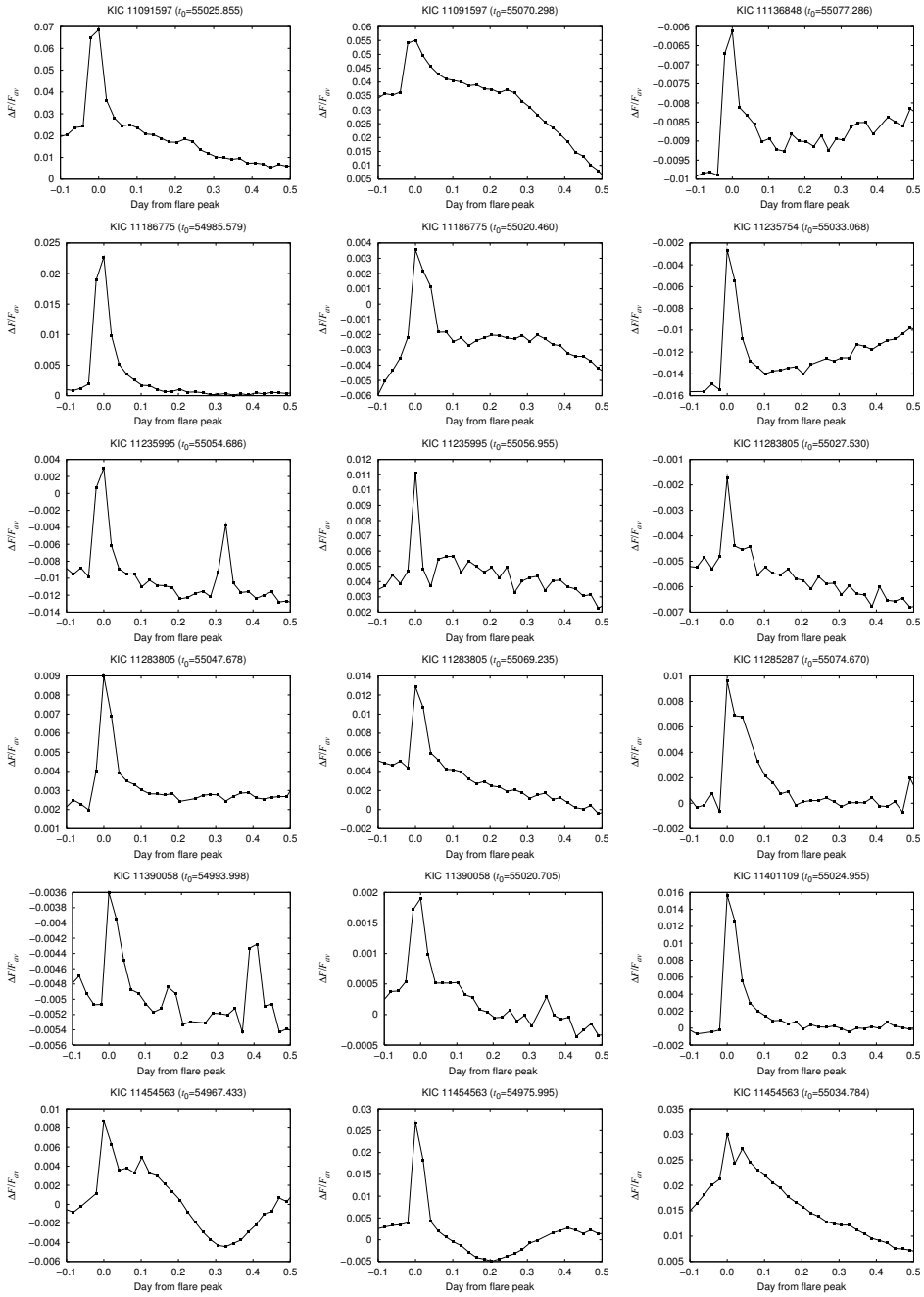

Figure S8: Light curves of each flare (cont.)

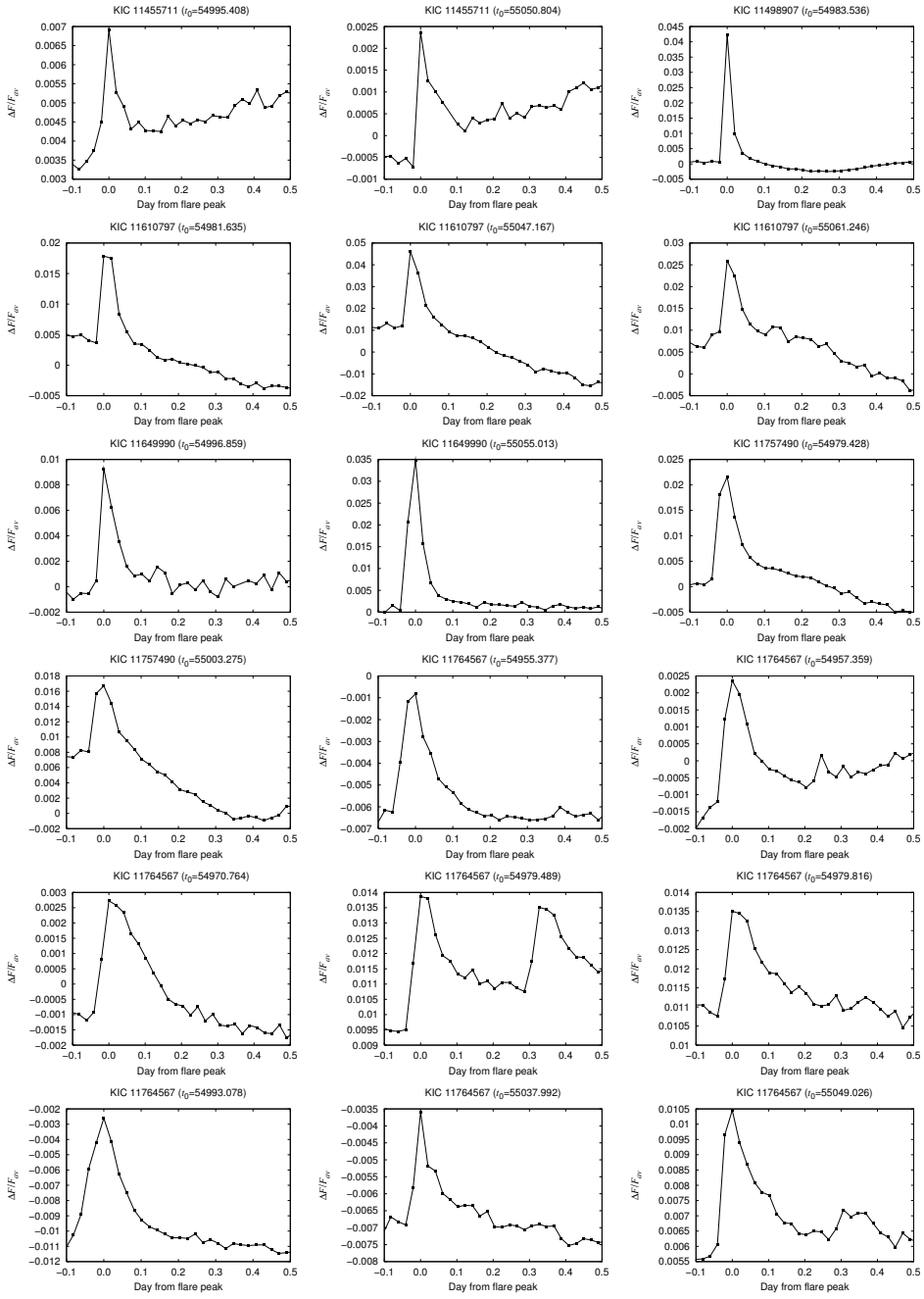

Figure S8: Light curves of each flare (cont.)

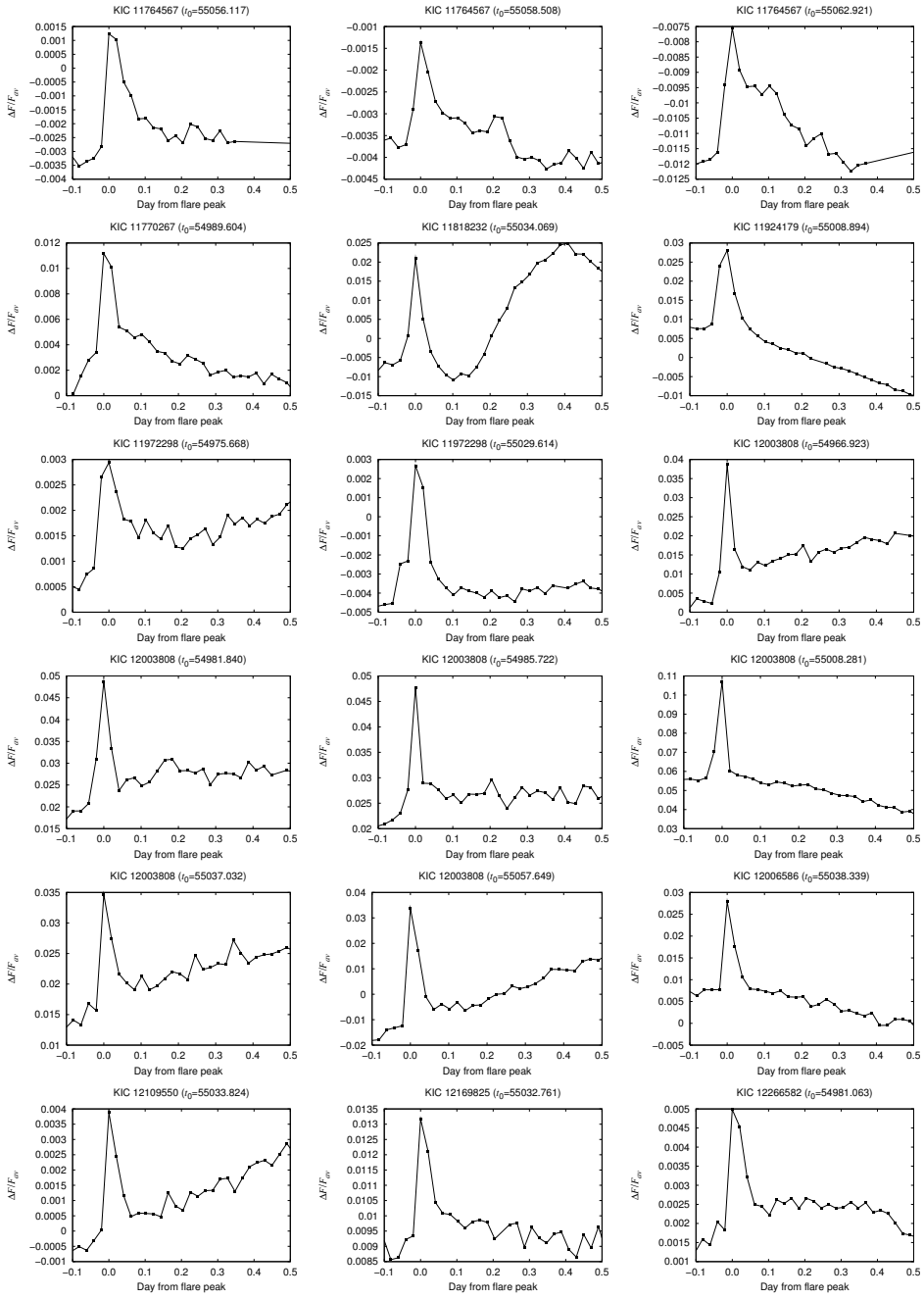

Figure S8: Light curves of each flare (cont.)

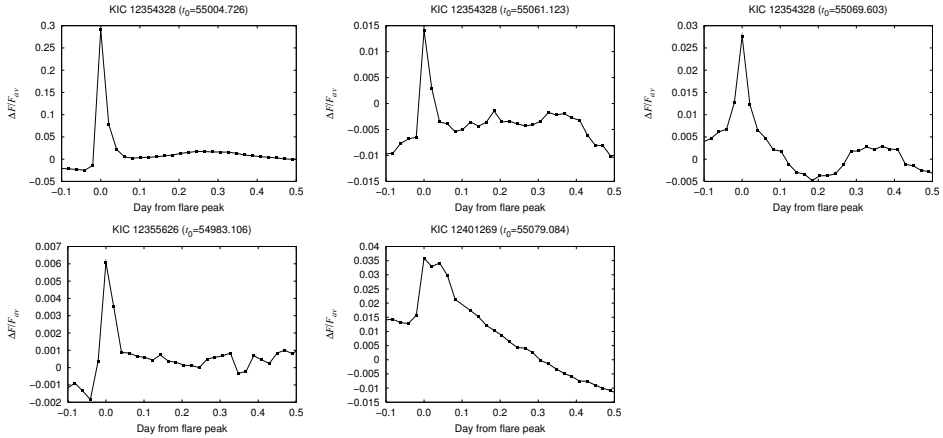

Figure S8: Light curves of each flare (cont.)